[AMERICAN JOURNAL OF SCIENCE, VOL. 298, JUNE, 1998, P. 441–470]

American Journal of Science

JUNE 1998

MODELING METAMORPHIC FLUID FLOW WITH REACTION—COMPACTION—PERMEABILITY FEEDBACKS

VICTOR N. BALASHOV* and BRUCE W. D. YARDLEY**

ABSTRACT. Existing models of metasomatic flow do not allow for the effect that reaction has on the flow patterns. Instead, it is assumed that the volatiles produced are negligible in volume compared to those infiltrated and that reaction does not modify permeability. This is clearly unlikely to be true for infiltration-driven decarbonation reactions.

The rates of porosity creation by reaction and porosity loss by creep have been calculated for a representative volume of calcite–quartz–wollastonite marble, and it is found that, even for a weak calcite matrix, the rate of porosity generation by reaction is likely to outstrip the collapse of porosity, as long as the system is out of equilibrium.

We have applied a self-consistent 1D finite-difference model to the reaction of calcite + quartz to wollastonite in a 10 m thick marble, in response to influx of H_2O rich fluid, with fixed boundary conditions. The model allows us to evaluate the effect of reaction on the porosity structure and fluid pressure variation across the layer, from which local Darcy fluxes can be evaluated. The progress of reaction that we model is constrained by hydrological considerations, with the requisite parameters recalculated as reaction progresses, assuming creep compaction of rock under the stress difference between lithostatic and fluid pressures.

We find that the volume of fluid released by decarbonation, driven by influx of H_2O, is sufficient to create a back-flow, so that further advancement of the reaction front is only possible as a result of diffusion of water against the Darcy flux. The effect of creep driven by differences between fluid pressure and lithostatic pressure is to reduce the permeability of the layer and especially reduce the secondary porosity developed in the zone at and behind the advancing reaction front. We predict that in a 3D situation, the porous zone of reacted marble becomes a conduit for layer-parallel flow, and the secondary porosity is infilled by calc-silicate minerals due to silica metasomatism.

LIST OF SYMBOLS

$A(\phi)$	porosity function in densification law, eq (24)
a^p	constant in the permeability eq (27)
C_k	molar concentration of kth component of fluid, k = 1, 2 (for CO_2 k = 1 and for H_2O k = 2)
D^0	mutual diffusion coefficient in binary mixture CO_2–H_2O
D_{Ca}	diffusion coefficient of calcium component in fluid
D^{eff}	effective diffusivity of silica through wollastonite layer
D_{GB}	grain-boundary diffusion coefficient
D^{eff}_{GB}	effective diffusivity of silica accordingly to grain-boundary diffusion
d_g	mean size of calcite grains
d_g^{Wo}	mean size of wollastonite grains
F	diffusion factor of the porous medium
f^r	general kinetic function, eq (11)

* Institute of Experimental Mineralogy of Russian Academy of Science, 142432 Chernogolovka, Moscow District, Russia.

** Department of Earth Sciences, University of Leeds, Leeds LS2 9JT, United Kingdom.

f^{cr} general creep function, eq (12)
H energy of activation in densification law, eq (24)
$\mathbf{i}_y$ unit vector for vertical direction.
g acceleration due to gravity.
j^r rate of chemical reaction
k^+ kinetic constant in eq (20)
k^p permeability of porous rock medium
L width of marble layer
L_{dif} diffusion length
M_k molecular mass of kth component, k = 1, 2
$\mathcal{M}_m^{Q_j}$ the mth mineral from paragenesis Q_j
m_{Si}^{Q} molality of silica in equilibrium with quartz
m_{Si}^{CW} molality of silica in equilibrium with calcite and wollastonite
m grain-size exponent in eq (24)
n stress exponent in eq (24)
P_f fluid pressure
P_f^0 fixed fluid pressure at inlet of marble layer
P_f^{fr} fluid pressure at the reaction front
P_f^L fixed fluid pressure at outlet of marble layer
P_l lithostatic pressure
Q energy activation for grain-boundary diffusion
Q_1 paragenesis of mineral products in reaction (1)
Q_2 paragenesis of mineral reagents in reaction (1)
q_- Darcy velocity on left of reaction front
q_+ Darcy velocity on right of reaction front
$\mathbf{q}$ Darcy velocity
R gas constant, 8.314 J/°K/mol
s_{Qtz}^0 specific surface area of quartz in marble
S_m concentration of mth mineral per unit volume of porous rock medium
S_{k-} concentration of kth component per unit volume of porous rock medium behind (to the left) of reaction front
S_{k+} concentration of kth component per unit volume of porous rock medium ahead (to the right) of reaction front
T temperature in °K
t, t^0 time and the initial time of process
V_m^0 molar volume of mth mineral
V_{Cal}^0 molar volume of calcite
$\overline{V}_k^0$ partial molar volume of kth pure component
$\overline{V}_k$ partial molar volume of kth component in CO_2–H_2O mixture
v^{fr} velocity of reaction front
W^r deviation from equilibrium for chemical reaction
X_k mole fraction of kth component in mixture, k = 1, 2.
X_{CO_2}, X_{H_2O} mole fractions of CO_2 and of H_2O in mixture
x space distance coordinate in the horizontal direction
x^{fr} the position of reaction front
ΔV_s^0 solid volume effect of chemical reaction
δ grain-boundary width
δD_0 pre-exponential term in eq (22)
ϕ porosity volume fraction
ϕ_m volume fraction of mth mineral

$\dot{\phi}^{cr}$ the rate of porosity loss due to creep
$\dot{\phi}_m^{cr}$ the rate of mth mineral volume fraction change due to creep
∇ gradient of variable
$\nabla\cdot$ divergence of flux
ν_k stoichiometrical coefficient of kth component in chemical reaction
$\nu_m^{Q_j}$ stoichiometrical coefficient of mth mineral of Q_j paragenesis in chemical reaction
ρ fluid density
ρ_{H_2O} water density in fluid CO_2-H_2O mixture
σ stress, MPa.
σ_{eff} effective stress or effective pressure, $\sigma_{eff} = P_l - P_f$
η fluid viscosity

INTRODUCTION

The significance of calc-silicate rocks and skarns as markers of fluid flow during metamorphism has been recognized for many years. While the general nature of the metasomatic processes involved has been understood for a long time (Korzhinskii, 1936, 1970; Thompson, 1959) and has been investigated experimentally (Zaraisky and others, 1986), sophisticated estimation of the quantities of fluid involved have been attempted only recently. Attempts to quantify fluid fluxes across lithologies in the metamorphic column have developed from simple analysis of stable isotope exchange between fluid and rock in a 1–D system, with local equilibrium and kinetic isotope exchange between fluid and rock along a flow path in which properties such as permeability are not affected by any metasomatic processes taking place (Bickle and McKenzie, 1987; Lassey and Blattner, 1988; Baumgartner and Rumble, 1988; Baumgartner and Ferry, 1991). However the development of experimental and theoretical investigations of mineral dissolution and precipitation rates and transport properties of rocks and fluids (Lasaga, 1981; Aagaard and Helgeson, 1982; Balashov and others, 1983; Lasaga, 1986; Murphy and Helgeson, 1987; Oelkers, 1988; Balashov, 1995; Zaraisky and Balashov, 1995; Oelkers, 1996) has provided a basis for a quantitative approach to chemical transport modeling, taking into account reaction kinetics (Lichtner, 1985, 1988; Lasaga and Rye, 1993) and feedback between reaction and porosity (Balashov and Lebedeva, 1991; Steefel and Lasaga, 1994; Steefel and Lichtner, 1994; Lichtner, 1996).

The importance of the deformation of rocks for the modification of fluid flow has been discussed by Knipe and McCaig (1994). One of the most fundamental ways in which deformation can influence fluid flow is through the modification of pore volume in response to changes in effective pressure: $\sigma_{eff} = \sigma_3 - P_f$. The relative simplicity of this physical basis does not imply simplicity in its general treatment when coupled with chemical reaction and mass transfer. Some aspects of this problem with extension to negative effective pressure in a viscous rock matrix have been addressed recently by Connolly (1997). The problem addressed here is, however, distinct: we are studying the potential of a specific lithological boundary for creating heterogeneities in permeability as a result of reaction that may then dominate fluid loss from surrounding rocks on a scale of hundreds of meters to kilometers, rather than the overall behavior of average crust.

In this paper, we model metasomatic processes in marbles, making specific allowance for the effect of fluid produced by decarbonation, enhancement of porosity by reaction and reduction of porosity by creep. Our ultimate aim is to evaluate the conditions under which impure marbles may become a focus for metamorphic fluid flow, which is a prerequisite for the development of calc-silicate skarns. In this paper we first evaluate the complex effects of reaction and stress on the porosity of a marble in which calcite and quartz are reacting to form wollastonite. The equations are then

incorporated into a 1-D flow model to evaluate the effect of decarbonation on transport and feedback. The results of the analysis are used to provide constraints on possible flow behavior and Si-metasomatism in a 2D and 3D environment without explicitly modelling Si-transport.

THE MODEL FOR REACTION AND FLOW

In this section we develop a general model for the flow of fluid into or out of a rock as a direct consequence of a reaction that releases volatiles. Contributions from both diffusive and advective mass transport are considered. The analysis is developed for a barycentric reference frame (de Groot and Mazur, 1984), that is one for which the net mass diffusive fluxes are zero, and which may therefore migrate relative to geological boundaries.

The master equations.–Consider an isothermal–isobaric system in which a generalized metamorphic devolatilization reaction takes place, leading to the replacement of the initial paragenesis Q_2 by paragenesis Q_1. We can write the reaction as:

$$\Sigma \nu_m^{Q_2} \mathcal{M}_m^{Q_2} \overset{k^+}{\rightleftharpoons} \Sigma \nu_m^{Q_1} \mathcal{M}_m^{Q_1} + \nu_1 CO_2 + \nu_2 H_2O, \tag{1}$$

where mineral $\mathcal{M}_m^{Q_j}$ belongs to paragenesis Q_j, i = 1, 2. The resulting changes in the amount and composition of fluid present in the rock (assuming complete miscibility) depend on the rate of movement of each fluid component into or out of the rock as a result of both advection and diffusion. This movement can be calculated using the independent component transport equations for a barycentric reference system, which define the balance between diffusive and advective flow and which have the form for a two-component system (Balashov and Lebedeva, 1996; see app.)

$$\frac{\partial \phi C_1}{\partial t} = \nabla \cdot \left(D^0 \frac{M_2}{\overline{V}_2} \frac{F}{\rho} \nabla C_1 \right) - \nabla \cdot (C_1 \mathbf{q}) + \nu_1 j^r$$

$$\frac{\partial \phi C_2}{\partial t} = \nabla \cdot \left(D^0 \frac{M_1}{\overline{V}_1} \frac{F}{\rho} \nabla C_2 \right) - \nabla \cdot (C_2 \mathbf{q}) + \nu_2 j^r. \tag{2}$$

Where the symbols are defined above in the List of Symbols, and the Darcy velocity, $\mathbf{q}$, is given by

$$\mathbf{q} = -\frac{k^p}{\eta} (\nabla P_f + \mathbf{i}_y \rho g), \tag{3}$$

The bulk fluid transport equation results from multiplying the component transport eqs (2) by the component masses, M_1 and M_2, and summing

$$\frac{\partial \phi \rho}{\partial t} = -\nabla \cdot (\rho \mathbf{q}) + j^r (\nu_2 M_2 + \nu_1 M_1). \tag{4}$$

This equation is valid for a barycentric reference system, defined as one for which $\Sigma M_k J_k = 0$, where M_k is the mass, and J_k is the diffusive flux of the k-th component.

Porosity evolution.–For a full description of the system it is necessary to include equations for mineral concentrations, taking into account the change in the total volume of each phase as reaction proceeds and the change in mineral mode as a fraction of the

total rock volume that results from elimination of porosity by compaction due to creep:

$$\frac{\partial \phi m}{\partial t} = V_m^0 \nu_m j^r + \dot{\phi}_m^{cr}. \tag{5}$$

Assuming deformation of the rock is dominated by homogeneous creep of the single most ductile matrix phase, with the relative proportions of minerals remaining constant, we obtain

$$\dot{\phi}_m^{cr} = -\frac{\phi_m}{\Sigma_m \phi_m} \dot{\phi}^{cr} = -\frac{\phi_m}{1-\phi} \dot{\phi}^{cr}, \tag{6}$$

making use of the relation between porosity and mineral volume fractions,

$$\sum_m \phi_m + \phi = 1. \tag{7}$$

Overall, the change of porosity with time in a rock undergoing reaction and compaction is given by:

$$\frac{\partial \phi}{\partial t} = -j^r \Delta V_s^0 + \dot{\phi}^{cr}, \tag{8}$$

where:

$$\Delta V_s^0 = \sum_m \nu_m V_m^0. \tag{9}$$

The first term of eq (8) defines the change in porosity due to reaction, and the second term, $\dot{\phi}^{cr}$, is the rate of porosity loss due to creep:

$$\dot{\phi}^{cr} = -\sum_m \dot{\phi}_m^{cr}. \tag{10}$$

The source function j^r in eqs (2), (4), and (5) is defined by a kinetic law that relates the rate of reaction to the degree of deviation from equilibrium (W^r)

$$j^r = f^r(W^r). \tag{11}$$

The rate of compaction with time, $\dot{\phi}^{cr}$, is defined by a deformation law and for the purposes of our analysis is simply a function of the difference between lithostatic pressure (P_l) and pore fluid pressure (P_f)

$$\dot{\phi}^{cr} = f^{cr}(P_l - P_f). \tag{12}$$

In general, f^{cr} should include a deviatoric stress component, but we assume that this is negligible relative to the effective pressure $\sigma_{eff} = P_l - P_f$. This is equivalent to the assumption: $\sigma_1 \approx \sigma_2 \approx \sigma_3 = P_l$.

Density–composition relations for binary CO_2–H_2O mixtures.–For the PT-conditions of the problem addressed here, we have ignored the volume of mixing term for CO_2–H_2O fluids and treated the partial molar volumes of fluid mixture components as equal to the molar volumes of the pure components (that is, $\overline{V}_k = \overline{V}_k^0$, $k = 1, 2$), taken from Shmulovich and Shmonov (1978).

The bulk fluid density is related to the volume concentration (mol/cc) of CO_2 in an H_2O–CO_2 fluid by the relation:

$$\rho = \left(M_1 - \frac{\overline{V}_1}{\overline{V}_2} M_2\right) C_1 + \frac{M_2}{\overline{V}_2}, \tag{13}$$

likewise, the mole fraction of CO_2 in the mixture is related to volume by:

$$X_1 = C_1 \frac{\overline{V}_2}{C_1(\overline{V}_2 - \overline{V}_1) + 1}. \tag{14}$$

The molar volume of a CO_2–H_2O mixture is defined as

$$\overline{V} = X_1\overline{V}_1 + X_2\overline{V}_2, \tag{15}$$

while the water density in the fluid grams cm^{-3} is

$$\rho_{H_2O} = M_2C_2 = M_2\frac{X_2}{\overline{V}}. \tag{16}$$

Because we consider only small variations in a fluid pressure relative to the 200 MPa mean pressure, we treat the fluid as incompressible.

APPLICATION TO A NATURAL METAMORPHIC REACTION

In this study we have taken the example of the well known metamorphic reaction

$$Cal + Qtz \overset{k^+}{\rightleftharpoons} Wo + CO_2 \tag{17}$$

occurring in a marble at 600°C and 200 MPa. This reaction was chosen because relevant data are available to evaluate both the reaction rate and the creep rate (Tanner, Kerrick, and Lasaga, 1985; Walker, Rutter, and Brodie, 1990; Zhang, Paterson, and Cox, 1994; Paterson, 1995), and also because it provides an extreme case of a very ductile rock due to the softness of calcite at such high temperatures.

The rate of generation of porosity.–The kinetics of reaction (17) were investigated by Tanner, Kerrick, and Lasaga (1985). We reinterpreted their experimental data on the basis of the extended kinetic-diffusion model of Lasaga (1986). The model includes two principal steps: diffusion of dissolved silica through the new-formed thin porous wollastonite layer to the calcite surface and formation of wollastonite on the calcite surface. Hence for any given X_{CO_2} we consider two principal chemical reactions:

$$Qtz \rightleftharpoons SiO^0_2, \tag{18}$$

$$Cal + SiO^0_{2,aq} \overset{k^+}{\rightleftharpoons} Wo + CO_2. \tag{19}$$

We assume that reaction (18) is at local equilibrium and the concentration of dissolved silica at the outer wollastonite surface is in equilibrium with quartz; the second reaction, (19), takes place on the calcite surface. Another simplification, valid for marble when the amount of calcite is much greater than that of quartz, is that the interface area between calcite and wollastonite is considered equal to the initial surface area of quartz in the rock. Accordingly, the model rate equation is formulated as

$$j^r = \frac{s^0_{Qtz}\tilde{\rho}_{H_2O}(m^Q_{Si} - m^{CW}_{Si})}{\left(\frac{1}{k^+} + \frac{\phi_{Wo}}{s^0_{Qtz}D^{eff}}\right)}, \tag{20}$$

where s^0_{Qtz} is the initial specific surface of quartz $cm^2\ cm^{-3}$ in the rock; $\tilde{\rho}_{H_2O} = \rho_{H_2O}/1000$; m^Q_{Si} and m^{CW}_{Si} are silica equilibrium molalities for reactions (18) and (19) respectively, at given X_{CO_2}; k^+ is the kinetic constant for reaction (19), $[s^{-1}]$; D^{eff} is the effective diffusivity of dissolved silica through the wollastonite layer, $cm^2\ s^{-1}$.

On the basis of experimental data at 800° to 850°C and 100 MPa from Tanner, Kerrick, and Lasaga (1985), we used eq (20) to determine the activation energy of reaction (19) to be 100.4 kJ $mole^{-1}$, and the effective silica diffusivity to be 10^{-8} cm^2/s. The estimated value of k^+ for 800°C and 200 MPa is $3.3 \cdot 10^{-5}\ s^{-1}$.

We can compare the estimated value of silica diffusivity with data of Joesten (1991) on grain-boundary diffusivity of silica in wollastonite rims. Accordingly to the grain-boundary diffusion mechanism the effective diffusivity D^{eff}_{GB} can be expressed as

$$D^{eff}_{GB} = \frac{2}{d^{Wo}_g}\delta D_{GB}, \tag{21}$$

where δ is the grain-boundary width, d^{Wo}_g is the grain-size of wollastonite, and D_{GB} is the grain-boundary diffusion coefficient. We can fit δD_{GB} to Arehnius law:

$$\delta D_{GB} = \delta D_0 \exp\left(-\frac{Q}{RT}\right), \tag{22}$$

where $\delta D_0 = 1.6 \cdot 10^{-10}\ m^3\ s^{-1}$, and $Q = 220$ kJ $mole^{-1}$ (Joesten and Fisher, 1988). Taking $d^{Wo}_g = 1$ μm (Tanner, Kerrick, and Lasaga, 1985) and making use of eqs. (21, 22) we found for D^{eff}_{GB} values of $6 \cdot 10^{-11}$ to $2 \cdot 10^{-10}$ cm^2/s in the temperature range 800° to 850°C. These values of diffusivity are too low in comparison to the experimental diffusivity ($10^{-8}\ cm^2\ s^{-1}$) which confirms that the reaction (19) is operated by diffusion of silica in an intergranular fluid rather than by grain-boundary diffusion.

Taking the calculated activation energy for reaction and the activation energy for diffusion of silica from Balashov (1995) we arrive at values of k^+ and D^{eff} at 600°C, 200 MPa of $2.5 \cdot 10^{-6}\ s^{-1}$ and $6 \cdot 10^{-9}\ cm^2\ s^{-1}$ respectively. These values were used in eq (20) during the further calculations of this study. The low silica diffusivity relative to diffusion in pore fluid (Balashov, 1995) corresponds to a diffusion factor across the wollastonite layer $\approx 10^{-5}$. This arises because silica diffusivity is for diffusion through a compact wollastonite layer around a quartz grain, not for diffusion through the porous bulk rock as a whole.

The variable W^r of eq (11) is represented in eq (20) by $(m^Q_{Si} - m^{CW}_{Si})$. The rate of porosity generation as a function of j^r can be written accordingly from (8)

$$\frac{\partial \phi^r}{\partial t} = -j^r \Delta V^0_{s,CQW}, \tag{23}$$

where $\Delta V^0_{s,CQW}$ is the ΔV^0_s for reaction (17). The rate of porosity generation at the zero moment of time $t = 0$, when reaction first starts, is presented as a function of X_{CO_2} in figure 1. The calculations were made using eqs (20) and (23). The initial abundance of quartz was taken as 9 volume percent. The equilibrium values for reactions (17, 19) are calculated from the SUPCRT92 data base and the Gibbs free energy of CO_2 (Shmulovich and Shmonov, 1978), assuming ideal mixing between carbon dioxide and water. The equilibrium value of X_{CO_2} at the chosen P-T conditions is 0.184. From figure 1 it is evident that the log rate of porosity generation (s^{-1}) varies rapidly with X_{CO_2} close to equilibrium, increasing to -7.7 at $X_{CO_2} = 0.16$, which is within one order of magnitude of the maximum value possible: -6.7 at $X_{CO_2} = 0$.

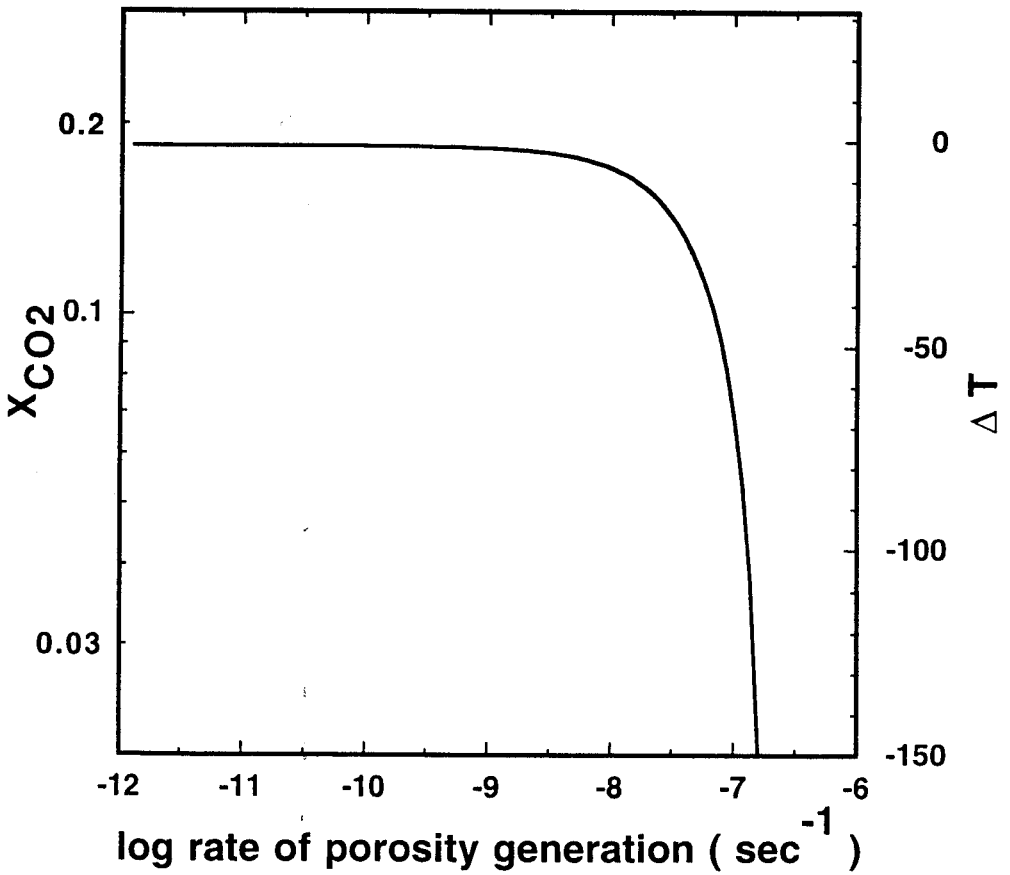

Fig. 1. Plot of the rate of porosity generation accompanying wollastonite growth through reaction (17), as a function of degree of overstepping at time t = 0. Overstepping is measured in terms of X_{CO_2} on the left hand axis and in terms of temperature on the right hand axis.

This calculation uses X_{CO_2} as a convenient measure of deviation from equilibrium. An alternative measure is the deviation of temperature from the equilibrium value for a given X_{CO_2}. The right hand side of figure 1 provides a calibration of the y axis in temperature terms, where ΔT is the deviation of the equilibrium temperature from 600°C corresponding to the overstepping indicated by the X_{CO_2} values shown on the left hand side. This shows that the major change in the rate of porosity generation is within 10° of equilibrium.

Marble compaction.–The rate at which marble compacts to eliminate porosity under the influence of an effective stress depends on the P-T conditions and the magnitude of the stress. Different deformation mechanisms dominate under different conditions and can be identified on a deformation mechanism map (Rutter, 1976). The general expression for a thermally activated deformation process is (Walker, Rutter, and Brodie, 1990):

$$\dot{\phi}^{cr} = A(\phi) \exp\left(-\frac{H}{RT}\right) \sigma^n d_g^m, \qquad (24)$$

where the energy of activation, H, the stress exponent, n, and grain-size exponent, m, vary between different deformation mechanisms.

For the P-T conditions considered here (200 MPa and 600°C), there are two relevant sets of experimental deformation data: hot isostatic pressing (HIP) of calcite aggregates (Zhang, Paterson, and Cox, 1994) and the grain-size sensitive flow of synthetic calcite rock (Walker, Rutter, and Brodie, 1990). In the first case argon was used as the pore fluid, and in the second case the samples were open to air.

The HIP data of calcite aggregates correspond to an activation energy, H = 390 kJ, stress exponent, n = 5, and grain-size exponent, m = 0. On the basis of the HIP data of Zhang, Paterson, and Cox (1994) we estimate the dependence of the function $A(\phi)$ on porosity over the range 0 to 0.08 to be:

$$A(\phi) = \exp(14\phi + 15). \tag{25}$$

Zhang, Paterson, and Cox (1994) found that the values of H and stress exponent n correspond roughly to the deformation of calcite aggregates by dislocation creep within

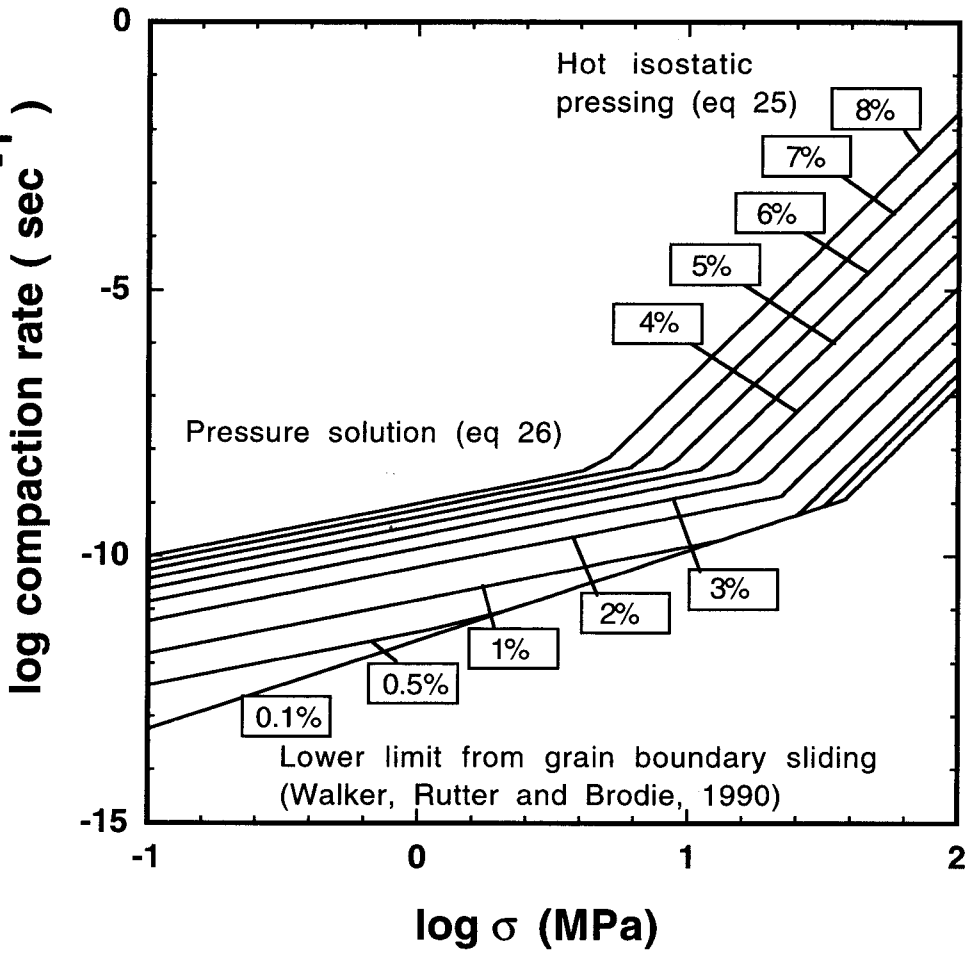

Fig. 2. Plot of the rate of porosity loss accompanying creep for coarse calcite marble, as a function of stress ($\sigma_{eff} = P_l - P_f$) at different porosity values. The different deformation laws, dominating in different parts of the diagram, are discussed in the text.

the grains and are higher than those found for diffusion controlled creep. These data apply to effective pressures $\sigma > 10$ MPa (Rutter, 1983) and were used to construct the high effective pressure part of the $\log \dot{\phi}^{cr} - \log \sigma$ diagram (fig. 2). This diagram should be considered as an isothermal cross section of a mechanical deformation map (Rutter, 1976).

The data on grain-size sensitive flow of synthetic calcite rock (Walker, Rutter, and Brodie, 1990) provide a limiting deformation rate for low porosity ($\phi = 0.1$ percent) and yield the limiting lower line on the left part of diagram. The line corresponds to the following parameters in eq (24): $A = 3 \cdot 10^{-4.9}$, H = 190 kJ, n = 1.7, and m = −1.9, where σ is in MPa and grain-size, d_g is in μm. These parameters are for aggregate deformation by grain-boundary sliding at low stresses ($\sigma < 25$ MPa). The multiplyer 3 in the pre-exponential term A represents transformation from uniaxial compression flow data to a volume compaction process. In our calculations the calcite grain size was set to 0.1 cm. For such a grain size the compression flow law with these parameters is only valid up to a rate of deformation of 10^{-9} s^{-1}. Hence the line we have shown is only approximate for the higher strain rate indicated here.

The presence of water-rich fluid must enhance grain-boundary sliding (Rehbinder and Shchukin, 1973), but nevertheless it is more important to take into account the influence of pressure solution on deformation of wet marble (Paterson, 1995; Rutter, 1983, 1976; Weyl, 1959). This mechanism of porosity reduction consists of three steps: dissolution of stressed material, transport through the pore fluid, and precipitation. Zaraisky and Balashov (1995) have shown that the interface term in the pressure solution equation can be ignored at high temperatures. Instead, the process is controlled by the diffusion step, for which we can write:

$$\dot{\phi}^{cr} = \frac{cFD_{Ca}V_{Cal}^2}{RTd_g^2}\sigma_{eff}, \tag{26}$$

where $c = (\rho_{H_2O}/1000)\,\overline{m}_{Ca}$, $\overline{m}_{Ca}$ being the calcium molality in the fluid in equilibrium with calcite, taken to be 0.05, and $\sigma_{eff} = P_l - P_{fl}$. The diffusion coefficient was taken from Balashov (1995), ($D_{Ca} = 4 \cdot 10^{-4}$ cm^2 s^{-1}). V_{Cal} and d_g are the molar volume, cm^3 $mole^{-1}$, and the calcite grain size, cm, respectively. The term F is the factor for intergranular pore diffusion and is given here as: $F = \phi^2$ (Paterson, 1995). Results from eq (26) show that, for the left hand region in figure 2, the pressure solution process is the predominant deformation process during compaction of marble.

Bulk creep model–rate of porosity generation versus rate of porosity loss.–An important consideration in evaluating how a reaction will develop in carbonate rocks, is the balance between porosity creation and porosity loss. Generation of metamorphic secondary porosity can lead to enhanced permeability, lowering of fluid pressure, and hence increased influx of non-chemically equilibrated fluid. This promotes further reaction, which thus becomes self-accelerating. On the other hand, if creep is sufficiently rapid to close pores faster than they grow, infiltration-driven reactions will slow down and stop.

Consider a bulk system at an initial time t^0 with a rate of porosity generation shown in figure 1. For a given initial porosity, any degree of reaction overstepping will lead to a rate of porosity generation that may be compensated by a stress value, σ, leading to an equal rate of porosity loss.

On this basis, the effects of both chemical reaction and compaction have been combined in figure 3, which shows fields of predominance of porosity generation and porosity loss at an initial time t^0. They are separated by a line we term here the Critical Initial Stress (CIS) Curve. The position of this curve is itself a function of porosity (hence the cluster of curves in fig. 3), and it marks the threshold between a field in which

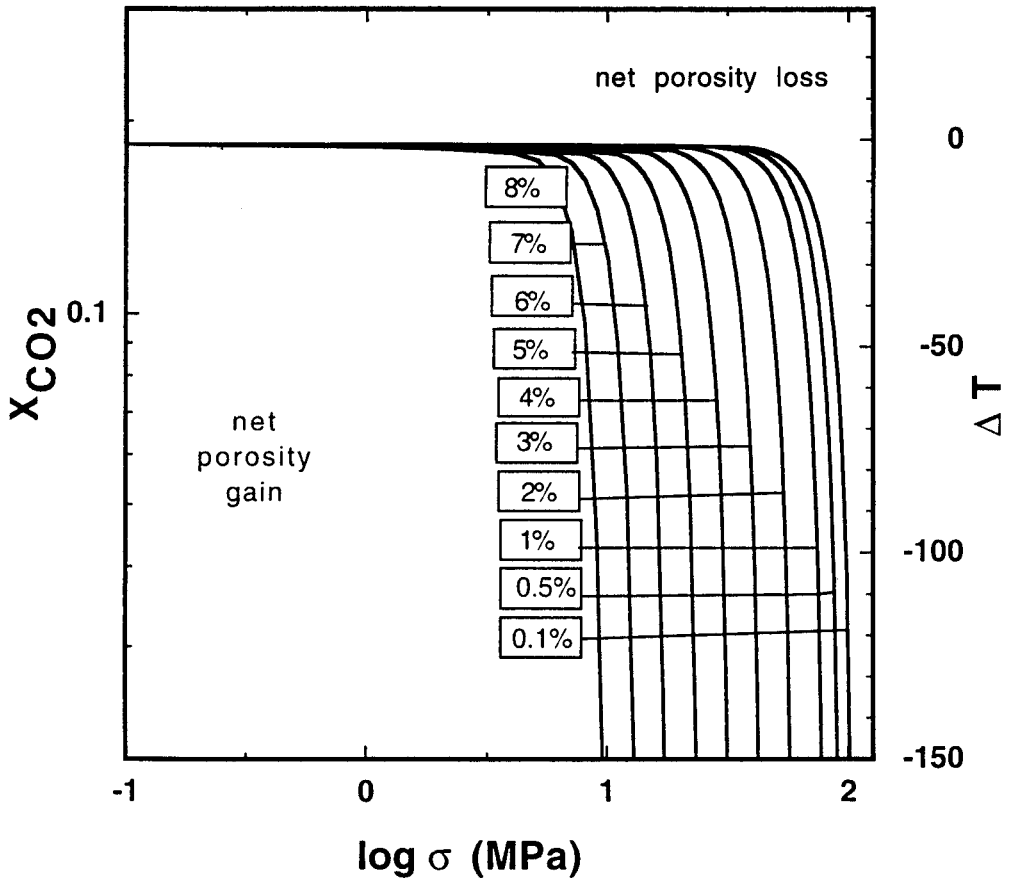

Fig. 3. Boundaries separating a field of net porosity increase from a field of net porosity loss, at various initial porosities, for a reacting calcite-quartz-wollastonite marble. Each curve is a Critical Initial Stress Curve for a specific initial porosity.

infiltration-driven reactions are likely to be self-accelerating and a field in which they will come to a halt.

Although figure 3 is calculated for t^0, the time at which reaction starts at any point in a marble, it is indicative of the behavior at subsequent times provided reaction (17) is still in progress. In detail, the rate of the metamorphic reaction will be slowed by the development of a rim of wollastonite armoring quartz grains, while the rate of porosity collapse will also decrease as the proportion of wollastonite to calcite increases. We have not attempted to quantify this effect.

The results shown in figure 3 are remarkable in that they show that appreciable porosities (several percent) may be maintained during reaction even when stresses are of the order of several hundred bars. This is in good accord with textural studies of calc-silicate rocks that illustrate growth into open porosity (Yardley and Lloyd, 1989).

COUPLED CREEP AND REACTION FLOW MODEL

The results presented in figure 3 are for a bulk system, and are of value in demonstrating the likely importance of porosity-generating reactions in calc-silicate rocks. However calc-silicate zones often develop at the edges of marble units, due to

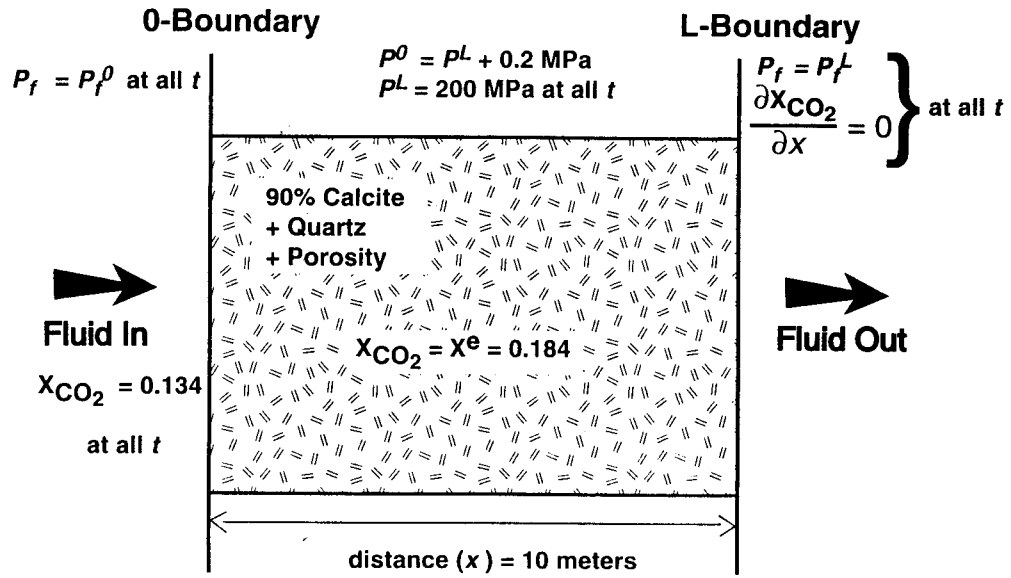

Fig. 4. Diagram to illustrate the 1-D marble layer modelled in the text, showing the composition and boundary conditions.

diffusion or infiltration of aqueous fluid components from adjacent siliceous rocks into the marble. As a next step to understanding this process, we evaluate here a 1-D model for infiltration-driven reaction, which takes into account the total fluid transport, including the effects of reaction and creep (fig. 4).

Rock permeability and porosity.–The permeability constant in Darcy's law (3) is defined by the geometrical structure of pore space and, hence, reflects the history of deformation, recrystallization, and pore fluid interactions. Although permeability is classically considered to be a rock property independent of fluid characteristics, this is no longer true for low porosity metamorphic rocks. The surface energy between mineral surfaces and pore fluid can dictate the manner and degree to which pores connect (Rehbinder and Shchukin, 1973) and hence controls the distribution of fluid along grain boundaries and the rock permeability (Holness and Graham, 1995). Experimental measurements of permeability as a function of temperature and effective pressure report a complex functional behavior with hysteresis phenomena (Shmonov, Vitovtova, and Zarubina, 1995).

To a first approximation, a cubic power law relationship between porosity and permeability:

$$k^p = a^p \phi^3, \tag{27}$$

has been found to be widely applicable to consolidated rocks (Brace, Walsh, and Frangos, 1968; David and others, 1994). This relationship is also incorporated into the Kozeny–Carman equation for porous media (Dullien, 1979).

Heating of rocks leads to thermal decompaction (dilation) as a result of the uneven expansion of the constituent mineral grains. Experimental studies of the increase in permeability due to thermal decompaction of rocks are in a good agreement with the relation $k^p \propto \phi_{th}^{\alpha}$, where α is slightly less than 3, and ϕ_{th} is the thermally induced porosity. Theoretical analysis on the basis of the percolation theory utilizing measured distribution of microcrack widths reveals that this relationship is due to the permeable pore network

being dominated by plane microcracks along grain-boundaries (Balashov, 1995; Zaraisky and Balashov, 1995). In contrast, the use of a capillary tube model would lead to a square power law for the permeability-porosity function which is not in agreement with experimental data.

Zhang, Paterson, and Cox (1994) found that the permeability of hot-pressed porous calcite aggregates follows the ϕ^3 law for $\phi > 7$ percent of porosity but at low values of porosity $k^p \propto \phi^{14}$. This was the result of the loss of connectivity between pores, and k^p remained proportional to the cube of the connected porosity at low values of ϕ.

For the specific reaction considered here (Tanner, Kerrick, and Lasaga, 1985; Lüttge and Metz, 1993) there are three possible effects of newly created porosity. If the grain size of both quartz and calcite grains is similar, and the modal percentage of quartz exceeds 15 percent (corresponding to the critical percolation threshold in a continuum model, Shklovski and Efros, 1975), the quartz grains become continuously connected giving rise to very high permeabilities as the porosity increases as a result of reaction. In this case, the exponent (α) in the power law relationship between ϕ and k^p is increased, $\alpha > 3$. On the other hand, if grain sizes are similar but there is <15 percent quartz, new pores tend to remain isolated giving rise to $\alpha < 3$, although the net volume increase resulting from the reaction eq (17), when the CO_2 is taken into account, means that porosity must connect at least transiently as fluid escapes. Finally, if quartz grains are significantly smaller than calcite grains, the newly created porosity will serve to enlarge the pores along the existing grain boundary structure, so that $\alpha \approx 3$.

The situation we have modelled corresponds most closely to the third case, and we therefore took the relationship eq (27) with a value of a^p of 10^{-12} m^2. Calculated permeabilities for marbles with porosities of 0.2 and 0.6 percent are $8 \cdot 10^{-21}$ and $2.2 \cdot 10^{-19}$ m^2. These compare very closely with measured permeabilities of marbles having these porosities, measured by Zaraisky and Balashov (1995), which were $1.3 \cdot 10^{-21}$ and $4.8 \cdot 10^{-19}$ m^2, respectively. We would emphasize however that the porosity-permeability relationships calculated here are intended to be illustrative rather than definitive. One of our main conclusions is that it is possible for porosity-creating reactions to generate zones of high permeability: if α is significantly greater than 3, the contrast in permeability between more porous and less porous rocks will be even more marked than we have assumed.

Formulation of the problem.–Consider a quartz-bearing marble in a vertical layer 10m wide undergoing formation of wollastonite by reaction (17) due to horizontal infiltration of $CO_2 + H_2O$ fluid through the layer under isothermal conditions of 600°C at 200 MPa. The boundary conditions are ($t \geq 0$)

$$x = 0 \begin{cases} X_1 = X_1^0 \\ P_f = P_f^0 \end{cases}, \qquad x = L \begin{cases} \dfrac{\partial X_1}{\partial x} = 0 \\ P_f = P_f^L \end{cases} \tag{28}$$

The initial mole fraction of CO_2 in the pore solution of the marble is the equilibrium value for reaction (17): $X_{CO_2} = 0.184$. The initial profile of fluid pressure through the layer is taken to be linear with boundary fluid pressures defined to support a pressure difference of 0.2 MPa, that is, $P_f^0 = 200.2$ MPa, and $P_f^L = 200$ MPa. This gives a fluid pressure gradient of 0.02 MPa/m which is set up to be comparable to a vertical lithostatic gradient in P_f.

The problem was solved for three possible regimes in the marble layer during decarbonation. The first case assumes that there is no compaction of pores in response to fluid pressure, we will refer to this case conventionally as to an absence of stress ($\sigma_{eff} = 0$). Note that this approach is normally adopted in reactive transport phenomena computa-

tions (Lichtner, Steefel, and Oelkers, 1996). In the second and the third cases we assume lithostatic pressure exceeds fluid pressure: $\sigma_{eff} = P_l - P_f^L = 1$ MPa and $\sigma_{eff} = 2.5$ MPa respectively. This assumption is crucial from a mathematical point of view because solutions of eqs (4), (12) that include negative effective pressures can give rise to the 'porosity waves' of Connolly (1997).

The calculations were made for two values of initial porosity: 1 and 0.1 percent. The initial calcite mode (volume fraction) was always 90 percent; the quartz mode was thus 9 or 9.9 percent according to the porosity value. The sizes of calcite and quartz grains were 0.1 and 0.01 cm respectively. The mutual diffusion coefficient in an H_2O–CO_2 fluid D^0, eq (2), and viscosity η, eq (3), were treated as constants equal to $7.1 \cdot 10^{-4}$ cm^2 s^{-1} and $7.3 \cdot 10^{-5}$ Pa s, respectively. These values were based on the data of Labotka (1991).

The important parameter that defines the diffusion or infiltration character for the initial rock transformation is the diffusion length of system

$$L_{dif} = \frac{D^0 \phi^0}{q^0}, \tag{29}$$

where ϕ^0 and q^0 are the initial porosity and the Darcy flux through the layer. The values of diffusion length for our porosity cases of 0.1 and 1 percent are 259 and 2.59 m respectively. It follows that for a fluid pressure difference 0.2MPa across rock layer 10m in width, the reaction is essentially driven by diffusion of fluid components. The solving of the general self-consistent model eqs (2, 3, and 5) makes it possible to take account of all these necessary factors in calculating the progress of reaction and infiltration. The system of differential equations with partial derivatives was solved using the finite difference method (Balashov and Lebedeva, 1996). In this study, however, rock deformation has been taken into account using eq (26).

Local equilibrium calculations.–For a better understanding of the space-time relations and the general direction of the process (Lichtner, 1993), we consider first the simplified, local chemical equilibrium solutions of the problem. For this, there are two limiting cases: pure infiltration and pure diffusion. In both cases $k^+ \rightarrow \infty$ and the reaction is concentrated at a sharp replacement front (Lichtner and Balashov, 1993). To find the limiting solution for infiltration, we ignore diffusion, that is, set $D^0 = 0$, and solve the equations:

$$a_- v^{fr} = -\frac{k_-^p}{\eta}\left(\frac{P_f^{fr} - P_f^0}{x^{fr}}\right)$$

$$a_+ v^{fr} = -\frac{k_+^p}{\eta}\left(\frac{P_f^L - P_f^{fr}}{L - x^{fr}}\right), \tag{30}$$

where v^{fr}, P_f^{fr} are the reaction front velocity and fluid pressure at the reaction front; the k_-^p and k_+^p are permeabilities to the left and right side of the front respectively, and the parameters a_- and a_+ relate the velocity of the fluid to that of the front on each side of it:

$$a_- = \frac{q_-}{v^{fr}}$$

$$a_+ = \frac{q_+}{v^{fr}}, \tag{31}$$

where q_- and q_+ are Darcy velocities on the left and right side of the front. The values of a_- and a_+ can be found by solving linear mass balance equations for the front (the Rankine–Hugoniot equations)

$$C_1^0 a_- - C_1^{eq} a_+ = S_{1-} - S_{1+}$$
$$C_2^0 a_- - C_2^{eq} a_+ = S_{2-} - S_{2+}, \tag{32}$$

where S_{k-} and S_{k+} are bulk concentrations of component k per unit volume of bulk porous medium (that is solid and fluid phases) to the left and right of the reaction front respectively. C^0 and C^{eq} are initial and equilibrium concentrations respectively.

The solutions of eqs (30) for the position of the reaction front through time are illustrated in figure 5. An important result of the pure infiltration model, which follows directly from (32), is that the value of the local equilibrium ratio of Darcy fluxes across the front: v_+^D/v_-^D, changes little with initial porosity, ranging from 1.0723 (4 percent porosity) to 1.0742 (0.1 percent porosity).

In the other endmember case, by ignoring the Darcy flux ($q = 0$) we can find the approximate diffusion solution by solving eq (33) for the first component (CO_2):

$$-D^0 \phi_- \frac{C_1^{eq} - C_1^0}{x^{fr}} = (S_{1-} - S_{1+}) \frac{dx^{fr}}{dt}, \tag{33}$$

where ϕ_- is the porosity of the newly forming layer. These results are also shown in figure 5 and are much less dependent on porosity. Porosities in excess of 1 percent are required for advection to predominate over diffusion over the 10 m thickness of the model system.

Based on the diffusion length of the system, we can expect that in the absence of rock compaction (at $\sigma_{eff} = 0$) the full solution (eqs 2, 3 and 5) for the moving reaction front will be near the pure diffusion case. At $\sigma_{eff} > 0$ the reaction front velocity will decrease. It is clear from figure 5 that advance of a reaction front through a 10 m thick layer will invariably be dominated by diffusion, unless large porosities (>1 percent) occur throughout the layer. The Darcy flux and the fluid pressure through the marble layer can be found only through solving the full equations system (eqs 2, 3, and 5). In further sections we consider our main results.

Porosity evolution.–Porosity increases markedly as wollastonite grows, tracking the advance of the reaction front (fig. 7A), but is lost by creep. Figure 6 shows porosity as function of distance in the direction normal to the marble layer at different times. Three different regimes of reaction and replacement are shown: for σ_{eff} values of 0, 1, and 2.5 MPa. The initial porosity was 1 percent. Reaction in the presence of compaction ($\sigma_{eff} > 0$) is characterized by curves with maxima that are located near the instantaneous reaction front and that decrease in magnitude with time. In this way the metasomatism of the marble layer is damped out by progressive compaction. A qualitatively similar result is obtained for an initial porosity of 0.1 percent.

Effect of stress on the advancing reaction front.–The effect of stress on the rate of advancement of the reaction front into the model marble is further illustrated in figure 7B and C. Increasing stress slows the progress of the reaction front but only slightly distorts the profiles of mineral modes (fig. 7B). Slowing the propagation of the reaction front during compaction limits the rate of change of fluid composition with time and has a significant effect on the profile of fluid composition (fig. 7C).

The position of the reaction front with time calculated from the solution of the full system of eqs (2, 3, and 5) together with limiting local equilibrium curves for propagation

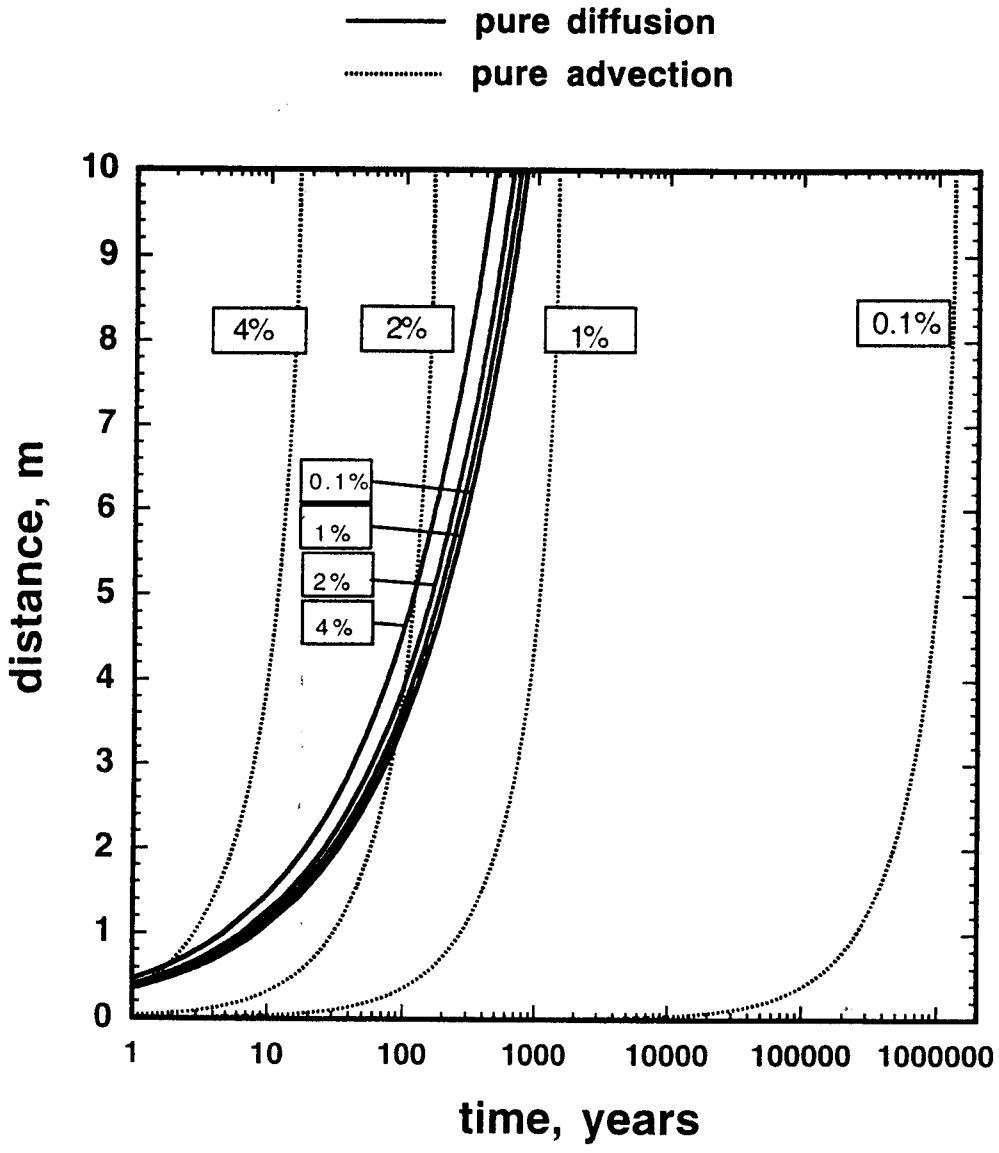

Fig. 5. Curves to illustrate the rate of advancement of the reaction front into the model marble layer, as a function of porosity, for the end member cases of pure diffusion and pure infiltration. Note that the advective case is much more dependent on porosity, and that except for rather large porosities, the front is likely to advance primarily by diffusion.

by pure diffusion or pure advection are depicted in figure 8. The calculations show a large velocity for the propagation of the reaction front, for example 2 m after 30 yrs with no compaction. The slowing of the front velocity with time reflects a diffusion dominated reaction progress. Allowing for creep due to differences between lithostatic and fluid pressures leads to significant slowing of the front (fig. 8) after the first few years, irrespective of initial porosity values.

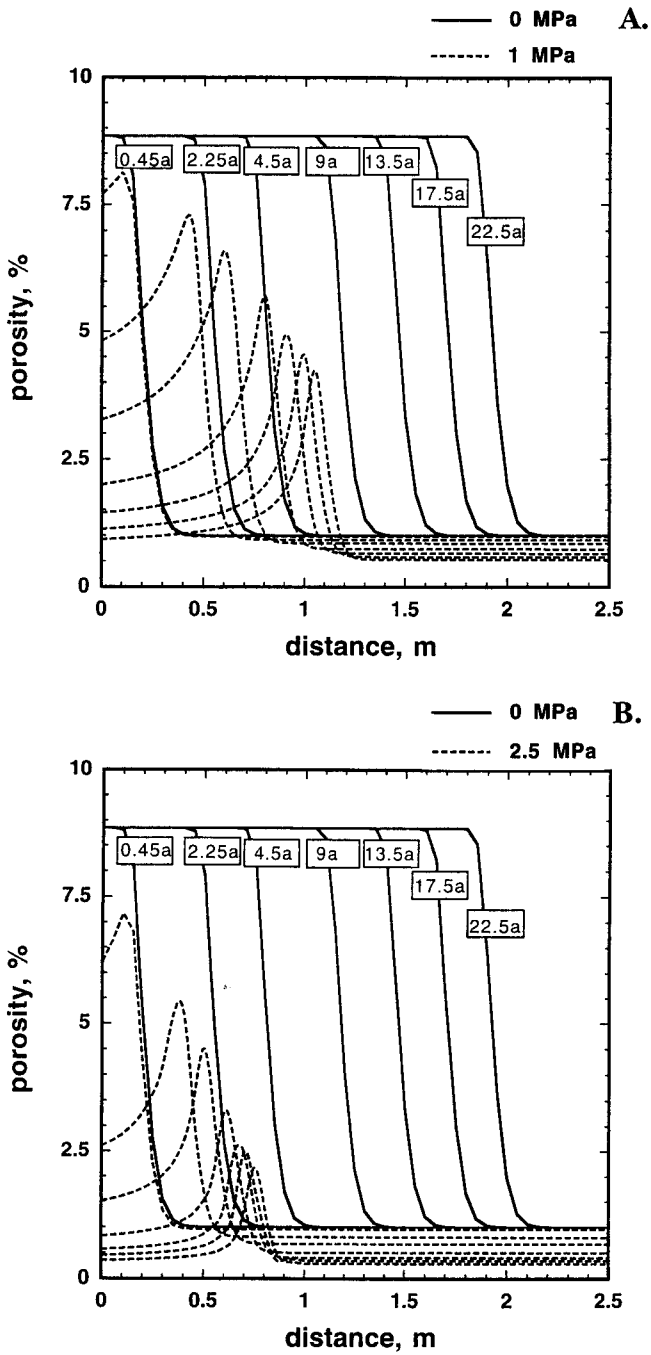

Fig. 6. The effects of compaction due to stress on the porosity profile generated across the advancing reaction front, at different times. (A) Stress (σ_{eff}) of 1 MPa contrasted with the stress-free case. (B) Stress (σ_{eff}) of 2.5 MPa contrasted with the stress-free case. Evident compaction of the unreacted marble is a consequence of the relatively high assumed initial porosity (1 percent).

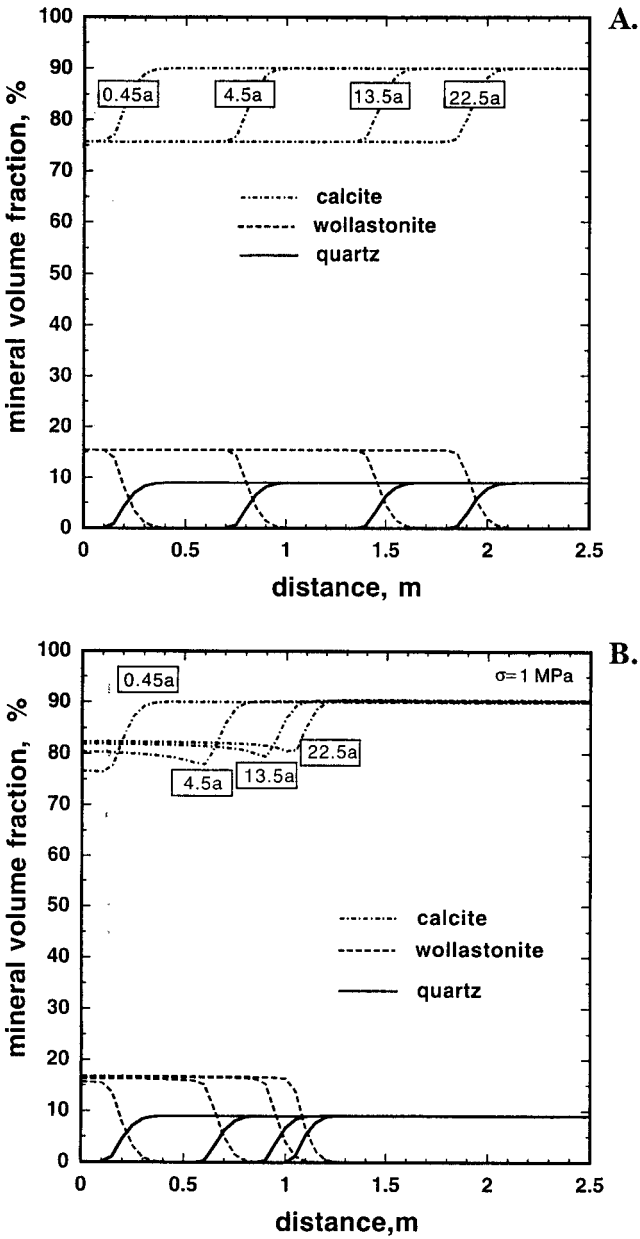

Fig. 7. Plots of the changes in mineral modes and fluid composition across the advancing reaction front at different times, for an initial porosity of 1 percent. These curves complement the porosity curves in figure 6A. (A) Changes in mineral modes in the stress-free case. (B) Changes in mineral modes in the presence of a 1 MPa stress.

Fluid pressure and flow.–Reaction (17) yields CO_2 which, from the master eqs (2 and 4), contributes to the Darcy flux of fluid. Figure 9A illustrates the distribution of fluid pressure inside the marble layer at $\phi^0 = 1$ percent, $\sigma = 0$ MPa. The corresponding fluid fluxes across the marble for different times are depicted in figure 10A. The initial reaction

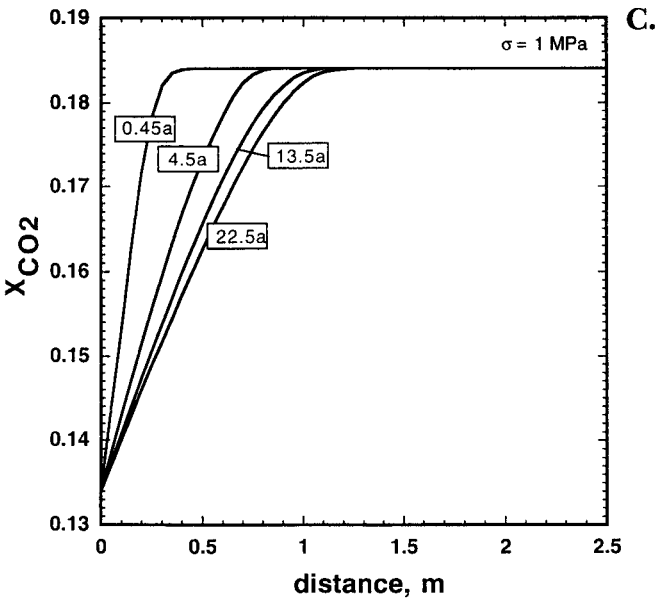

Fig. 7(C) Variations in fluid composition between the initial value and the infiltrating composition, also for the stressed case.

generates sufficient fluid for the fluid pressure at the reaction front to exceed the maximum initial pressure at the boundary, P_f^0, and as a result the flow is reversed behind the front, due to a maximum in fluid pressure at the reaction front illustrated in the inset to figure 9A. The reaction front continues to advance but is driven by diffusion: the diffusive flux of water, less the Darcy flux of water behind the reaction front is equal to Darcy flux of water ahead of the reaction front. With time the intensity of the back-flow decreases, then disappears after 17.5a (fig. 10A).

The effect of reducing the initial porosity from 1 to 0.1 percent results in a circa 100-fold increase in the maximum of fluid pressure (fig. 9B). The low initial porosity significantly decreases the fluid flux through the marble layer in the positive direction (fig. 10A), and the marble is practically impermeable. For this reason, where the initial porosity is very low, metamorphic reaction within the layer is dominated by reversed fluid flow.

Applying a stress so that marble compacts leads to more complex patterns of fluid pressure in space and time (fig. 9C).

The Darcy velocity for fluid ahead of the reaction front (fig. 10) is a function of porosity. In the case of a compacting system, progressive reduction in porosity with time leads to a marked decrease in velocity with time compared to the unstressed case (fig. 10B). In general, the effect of compaction by creep is to cause an increase of fluid pressure within the layer. This effect is a consequence of the power law used for permeability ($\propto \phi^3$), the amount of fluid leaving the marble is approximately linearly dependent on porosity.

An important numerical result is our finding that back-flow of fluid occurs for all initial conditions of stress with marble porosity <2 percent and has a very similar velocity, about 0.01 to 0.1 m/a, for the first few years (figs. 10 and 11). This circumstance is a consequence of the chemical reaction, which continues to be driven by diffusion against the advective flux.

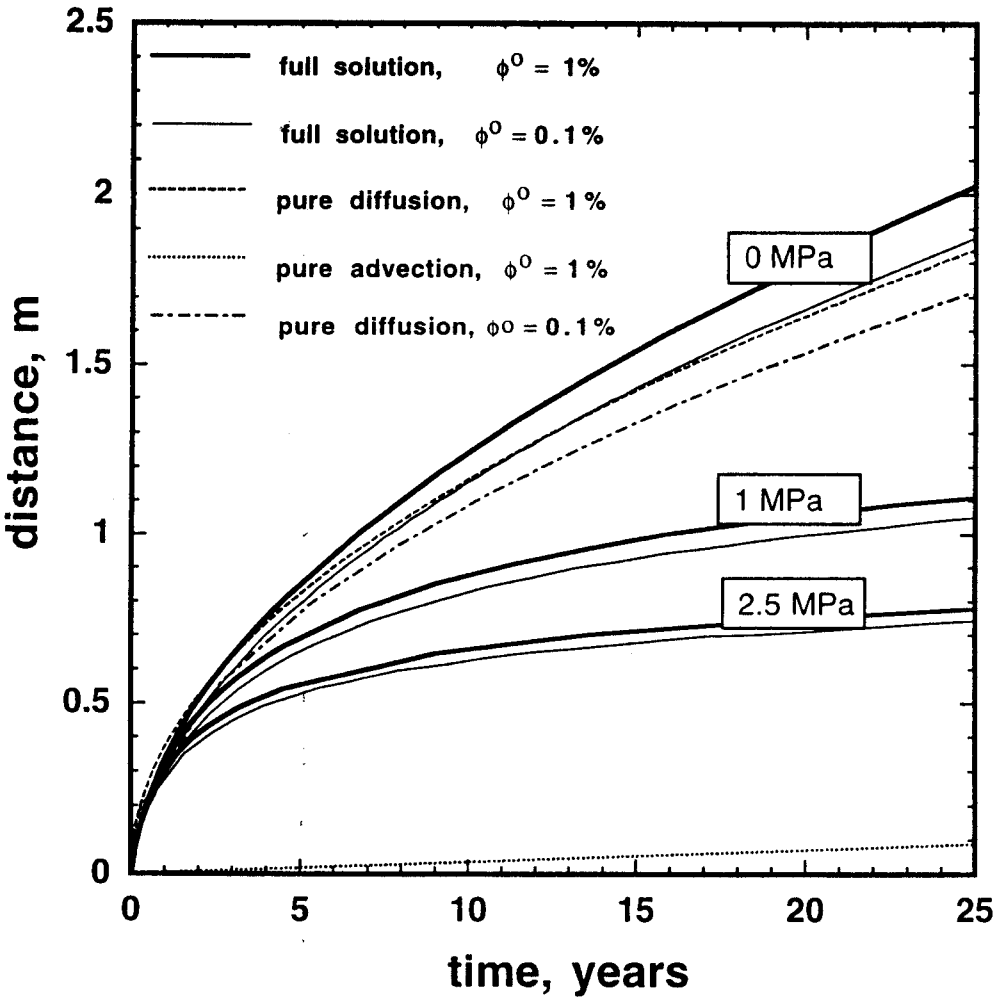

Fig. 8. Curves to illustrate the initial advancement of the reaction front (compare fig. 5, note the different time axis) into a marble with 1.0 or 0.1 percent initial porosity, for various stresses. Note the distinctly greater rate of advancement obtained from the full solution of the transport equation compared to the results for the endmember processes, despite the apparently negligible rate of advancement by pure advection.

'Reactive' values of X_{CO_2}.—For compacting systems the relationship between porosity and X_{CO_2} always exhibits a porosity maximum (fig. 12), and this occurs at a value of X_{CO_2} which lies below the equilibrium value. We can consider the X_{CO_2} value at which this maximum occurs as representing the average degree of overstepping of the reaction for a given time. As time progresses, the porosity at the maximum decreases, while the corresponding value of X_{CO_2} approaches the equilibrium value. From figure 12 it is apparent that the curves of porosity maxima all lie under the stationary line of balanced gain and loss of porosity in the bulk model, defined in figure 3. Hence the porosity–X_{CO_2} function in the chemical transport model always lies within the field of net porosity gain defined in the simple bulk model.

IMPLICATIONS FOR NATURAL FLOW AND SKARN FORMATION

A key feature of the results is the importance of diffusion rather than infiltration in advancing the reaction front. The generation of carbon dioxide at the reaction front effectively reverses the direction of fluid flow during the early stages of the reaction history, (fig. 11) and prevents further fluid flow into the marble. Only where the initial porosity in the marble is very large (>2 percent) is advective transport likely to dictate the migration of the reaction front into it, at least over length scales of a few meters. In practice, large porosities, and hence advective advancement of the reaction front, are only likely to occur where a thermally-driven decarbonation reaction has created a pervasive secondary porosity throughout the marble unit as a whole.

Because the movement of the front is normally diffusion controlled, it becomes possible to extrapolate with more confidence to 2- or 3-dimensions. Assuming the marble layer is not perfectly horizontal and uniform, then variations in hydraulic head will arise along it, as a result of which fluid will flow through the outer, reacted part. Thus layer parallel focussed flow through the high porosity zone will be accompanied by slow, diffusion-controlled migration of the permeable zone further into the marble. In this way, the reaction front, is a "metasomatic side" (Yardley and Lloyd, 1995), with respect to advection, since it is parallel to fluid flow, but nevertheless propagates as a result of diffusion at right angles to the front (Blattner and Lassey, 1990). The main constraint on the fluid flux through the 1-D model considered here is the low permeability of the unreacted marble; however, in a natural situation permeability of marbles is likely to be even lower, resulting in even less advection through the marble.

Silica metasomatism accompanying marble reactions.–In a 3D situation, further production of wollastonite from calcite may take place in the permeable zone behind the reaction "front" through reaction (19), here driven by introduction of silica in solution flowing along the porous zone, sourced from adjacent schists. Unlike reaction (17), reaction (19) leads to an increase in solid volume and a reduction in porosity equivalent to 7.5 percent of the volume of the calcite that is consumed. In calc-silicate skarn layers at the edges of marbles, it is commonly the case that no carbonate remains, and hence the porosity generated by quartz-based decarbonation reactions, such as (17), must have been sufficient to accommodate the increase in solid volume accompanying complete carbonate breakdown by metasomatic silica introduction, as in reaction (19).

For our model composition of marble, the amount of porosity that must be present for total conversion of the remaining calcite to wollastonite by silica metasomatism is 6.14 percent. In the presence of an effective stress, which is inevitable in a high-flow regime, it is clear from figure 6 that such a large porosity is most likely to be obtained near the edge of the layer. We have plotted the locus of the maximum porosity attained at any time as a function of distance, for stresses of 1 and 2.5 MPa, in figure 13. Assuming that the layer parallel flow is sufficiently extensive for reaction not to be limited by silica supply, it can be seen that pure wollastonite skarns will be restricted to the outermost tens of centimeters of the reacting layer. In the higher stress case it is clear that only the outermost metre of marble is likely to be metasomatized at all. Thus porosity-forming reactions in the interior of a marble are unlikely to lead to large scale fluid influx, but when they occur near the margins, extensive flow of fluid derived from adjacent lithologies may be focussed through the zone of reaction causing silica metasomatism. This helps explain the common development of calcsilicate rocks at the margins of amphibolite facies marbles. In this study, we have investigated the consequences of initiating a porosity-creating reaction in the outer part of a marble as a result of infiltration of non-equilibrium fluid. Similar effects may also result if the creation of porosity is the result of decarbonation due to increased temperature, rather than

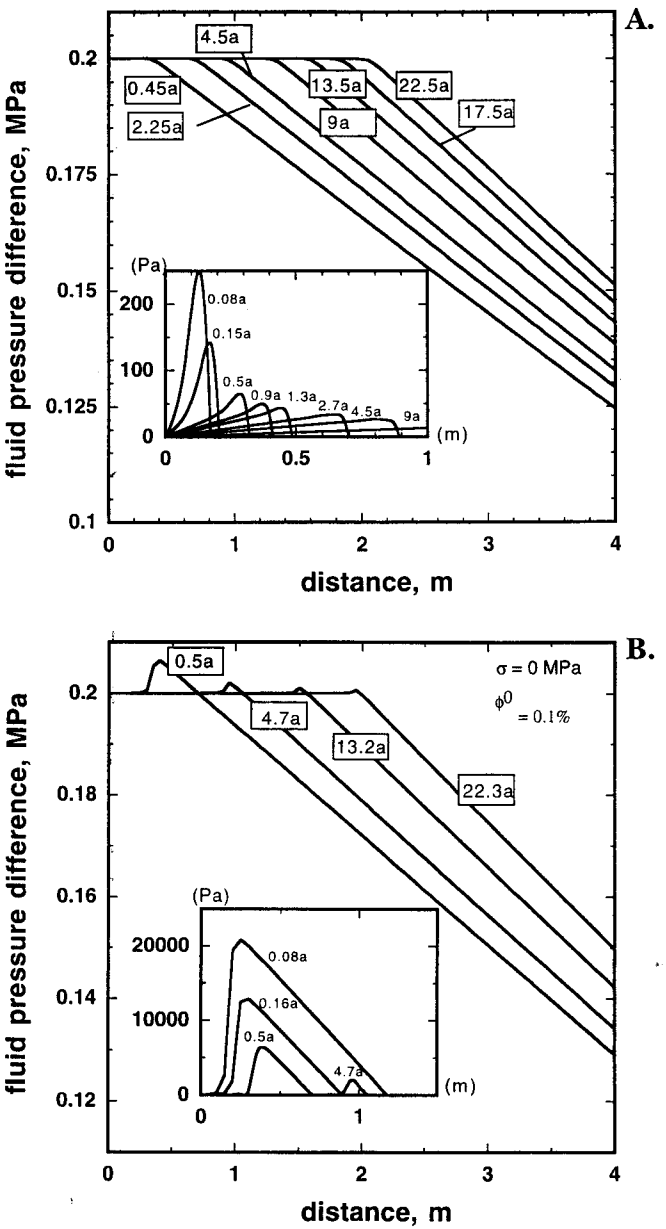

Fig. 9. Changes in fluid pressure across the reaction front in the model marble layer, at a series of times. The pressure axis shows the amount by which the fluid pressure exceeds 200 MPa, the boundary pressure on the right. The details of the initial build up of high fluid pressure at the reaction front, leading to back-flow as well as forward-flow from the site of reaction, are shown as insets. These are labelled with the fluid pressure in excess of 200.2 MPa, the boundary pressure on the left. (A) Initial porosity 1.0 percent, no compaction. (B) Initial porosity 0.1 percent, no compaction.

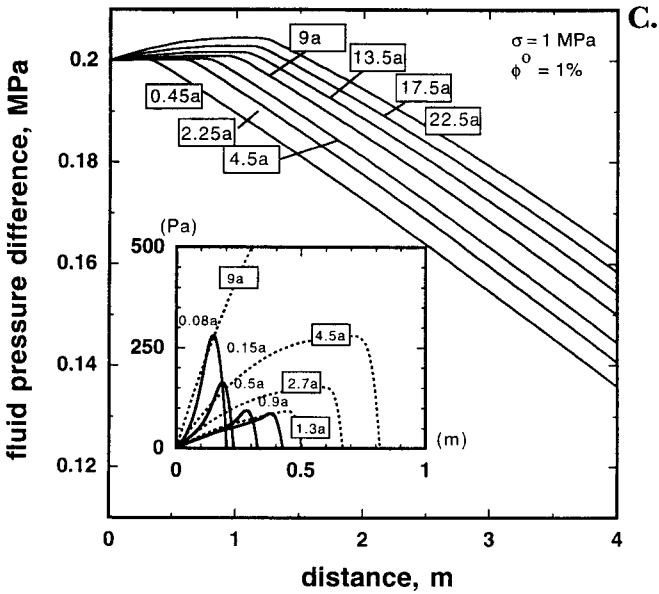

Fig. 9(C) Initial porosity 1.0 percent, compaction occurring in response to a stress of 1 MPa.

to infiltration, even though in this case the porosity will initially be distributed through out the marble layer, rather than localized at the margins. As in the case modelled here, the effect of a thermally activated increase in porosity and permeability will be to focus flow of fluid into the reacting layer, and this is likely to introduce non-equilibrium fluid into the reacted marble. This fluid, assuming it is relatively water-rich, will cause the decarbonation reaction to be even more strongly overstepped as it enters the margins of the marble, leading to an increase in the porosity and in the amount of infiltration. Such effects will be diminished further into the marble, since the fluid will be progressively equilibrated, so that extreme metasomatic changes (skarn formation) are likely to be restricted to the outer part of the marble.

CONCLUSIONS

In this study we have attempted to model metamorphic fluid flow through marbles, taking into account both their reactivity and their rheological properties under medium to high grade metamorphic conditions. The modelling demonstrates that the progress of infiltration- and diffusion-driven decarbonation reactions is influenced significantly by the generation of fluid and porosity during the reaction. The volume of fluid released by decarbonation is a significant part of the total fluid budget and results in an appreciable flow against the overall infiltration direction during the early stages of reaction, which nevertheless continues to advance because of diffusion of water against this flow. Porosity is generated rapidly by decarbonation for quite small degrees of overstepping, causing enhanced permeability behind the reaction front. In a 3-D situation, this zone of enhanced permeability will provide a channelway for fluid advection parallel to the reaction front, even though the front itself advances by diffusion.

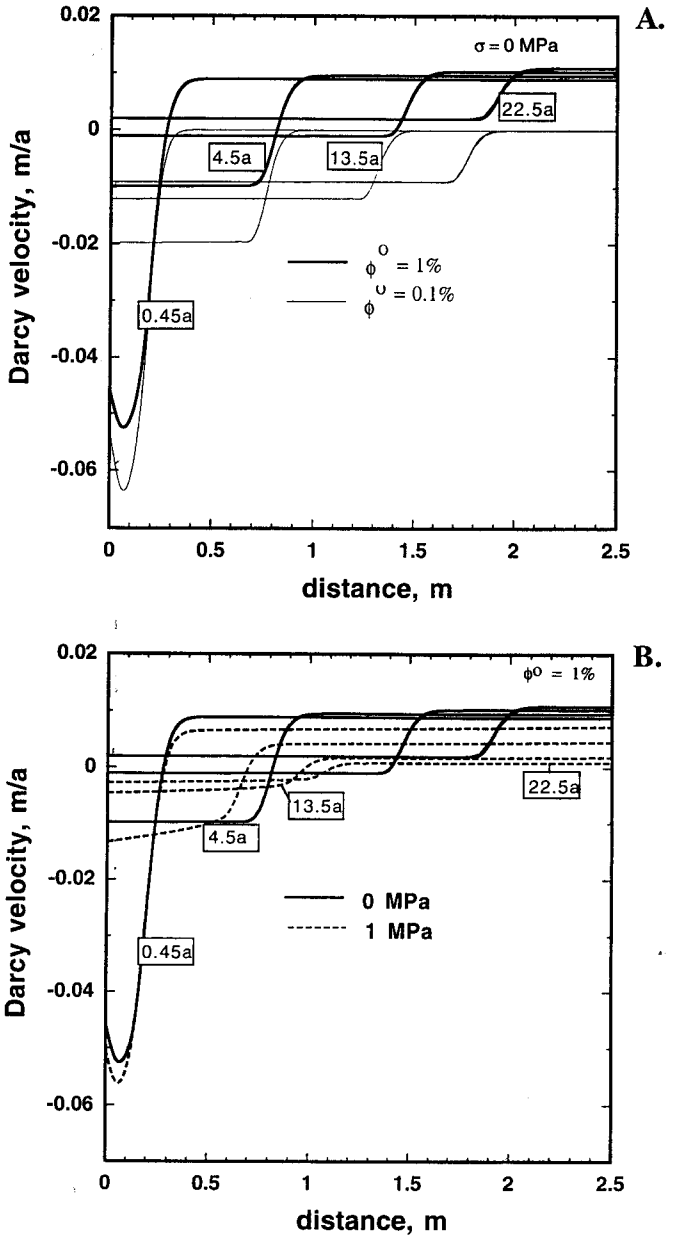

Fig. 10. Changes in the Darcy velocity of pore fluid across the reaction front in the model marble layer. Negative values denote back-flow (that is, to the left in the model illustrated in figure 4. (A) Unstressed case, note the greater back-flow in the case of the lower initial porosity value (0.1 percent). (B) Marble with an initial porosity of 1.0 percent showing the effects of a stress of 1 MPa, which has the effect of lowering the porosity throughout the marble.

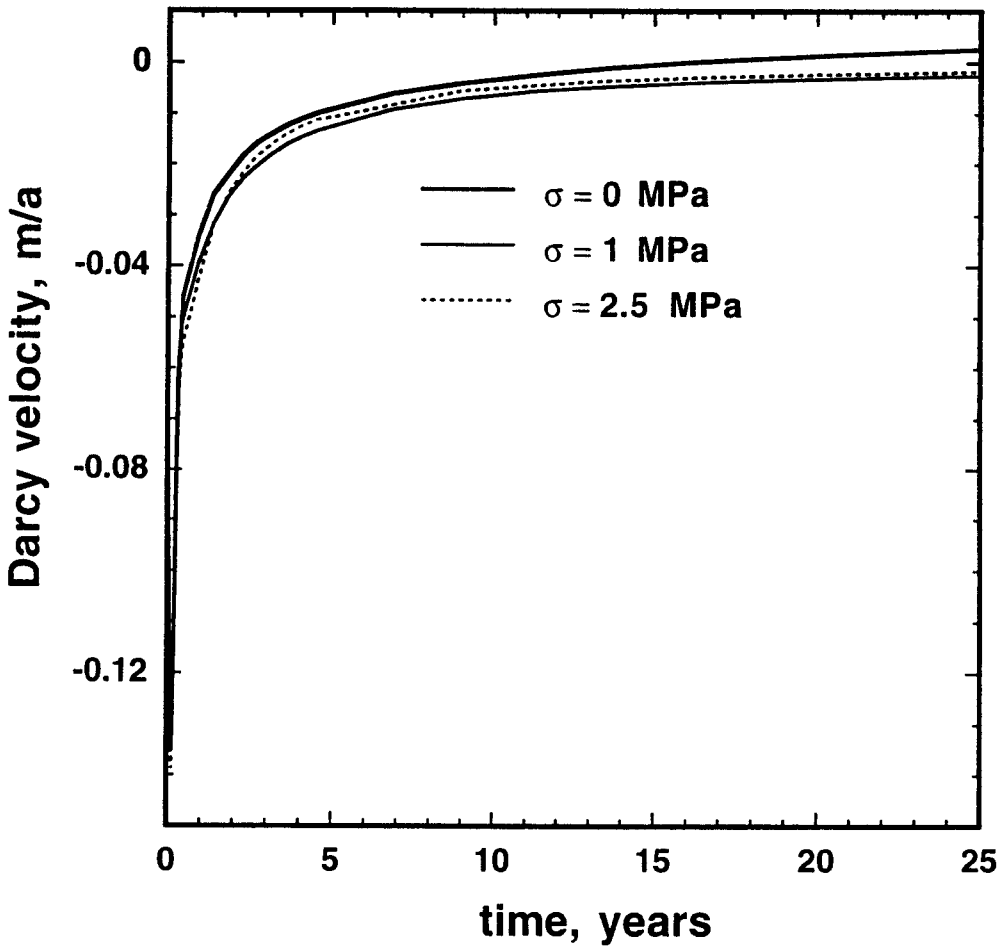

Fig. 11. Plot of the reversed flux obtained at inlet (x = 0) across a marble with initial porosity 1.0 percent (fig. 10B) as a function of time. Note the rather minor effect of stress.

The effect of enhancement of permeability due to decarbonation will be to lower fluid pressure, creating an effective stress (the difference between fluid pressure and lithostatic pressure). Relatively small values of stress of about 1 to 2.5 MPa have a significant effect on the reaction progress, because porosity loss by creep dampens out the infiltration-driven metamorphic process. Nevertheless, in the case of formation of wollastonite from calcite and quartz in a marble, the chemical reaction rates are sufficiently fast to maintain relatively large volumes of secondary porosity (several percent) against creep while the reaction is proceeding (that is, over times of tens of years at any point).

The reaction that we have analyzed will produce a wollastonite marble but not a calc-silicate skarn, which requires metasomatic addition of silica via the fluid. In 2D or 3D, layer-parallel flow through the porous wollastonite-bearing layer will introduce quartz-saturated fluid from adjacent schists (Yardley and Lloyd, 1995), and this can lead to the formation of monomineralic wollastonite skarn. The formation of wollastonite

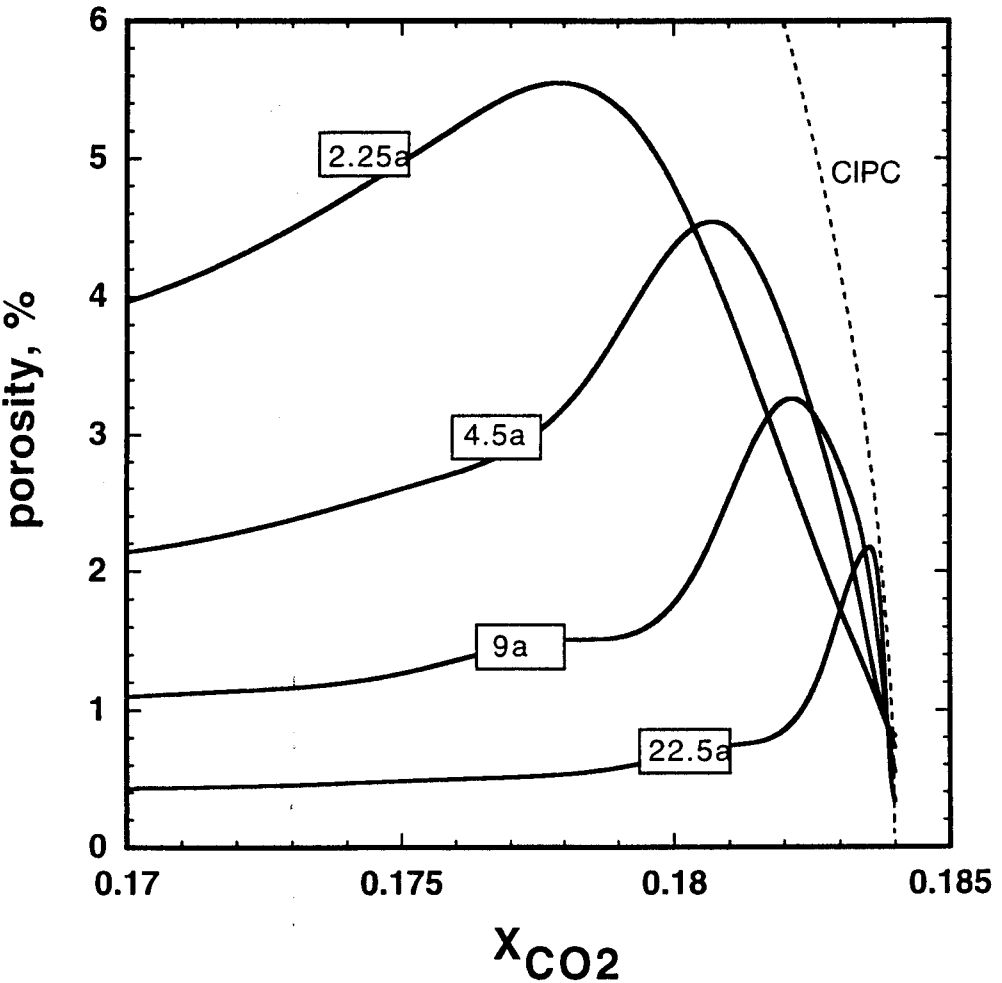

Fig. 12. Variation in X_{CO_2} with porosity across the reaction front, for an initial porosity of 1.0 percent and a stress of 2.5 MPa. The equilibrium value of X_{CO_2} is 0.184, and the curve labelled CIPC is the Critical Initial Porosity Curve, defining the maximum porosity at any given X_{CO_2} for which the rate of porosity generation by reaction will exceed the rate of porosity loss by compaction (fig. 3). Note that all the model porosity $-X_{CO_2}$ curves lie in the field of spontaneously increasing porosity.

from calcite by silica metasomatism infills porosity and so is only likely to go to completion in the outermost parts of the original marble layer. As the reaction front moves into the marble, the effect of creep is to reduce the maximum porosity attained. Although our modelling is based on a metasomatic process triggered by infiltration, qualitatively similar metasomatic effects are likely if decarbonation is initiated by thermal overstepping, although in this case some reaction products will form throughout the marble.

The modelling carried out here shows that overstepped decarbonation reactions proceed very rapidly relative to the overall duration of even a contact metamorphic event and have the potential to focus fluid flow from a large volume of metamorphic rocks through narrow skarn layers. It is, therefore, likely that skarn-forming processes

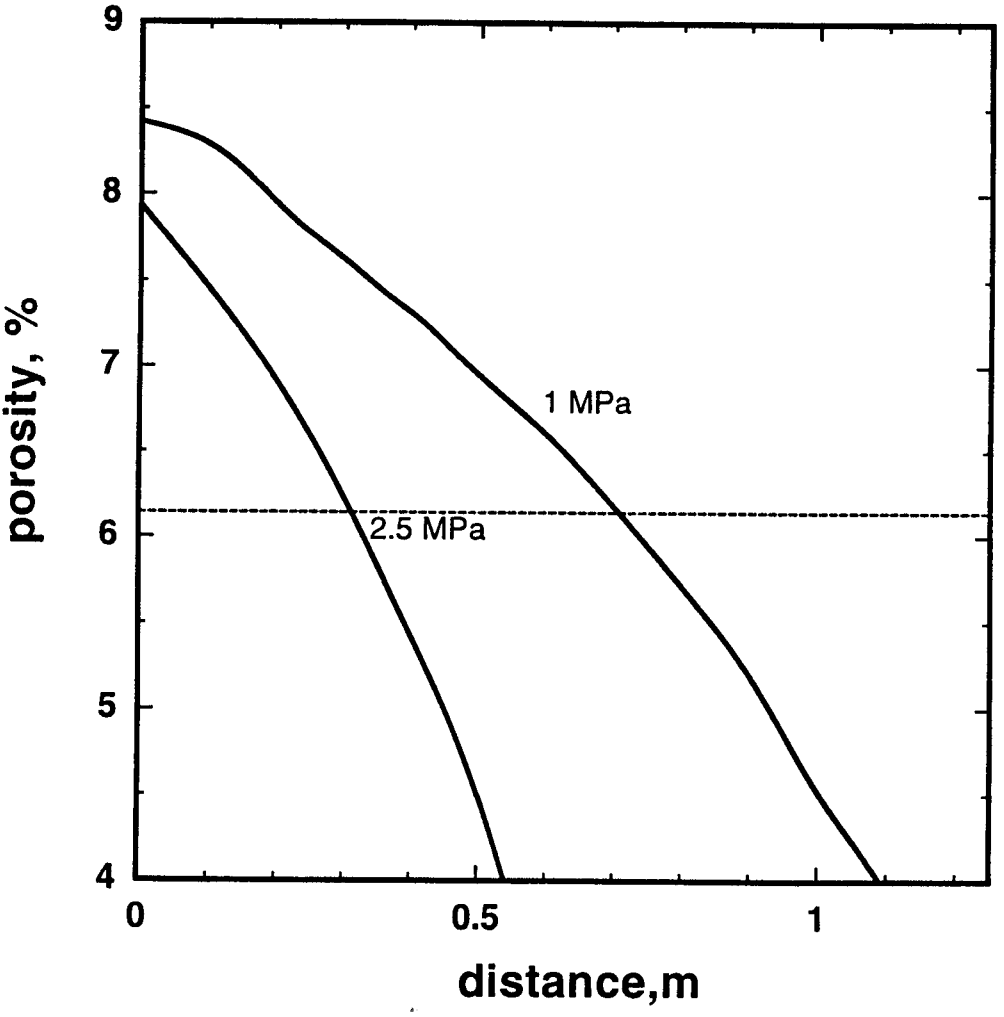

Fig. 13. Plot of the maximum porosity obtained near the reaction front as a function of distance (and hence time), extracted from figure 6, for stress values of 1 and 2.5 MPa. The horizontal line defines the minimum porosity required for all the remaining calcite in the marble to be converted to wollastonite by metasomatic introduction of silica, to accommodate the increase in volume of reaction (19). Note that if silica availability is not the rate-limiting factor, the formation of a pure calc-silicate skarn as a result of layer-parallel flow along the reacted porous margin of the marble, is still limited to the outermost few 10's of cms.

around marbles play a much more important role in the release of fluid from medium to high grade metamorphic belts than the volumetric abundance of skarns would suggest.

ACKNOWLEDGMENTS

This work has been supported by the Royal Society through a Joint Project visit, ex-quota visit by Dr. Balashov to Leeds, and by Russian Basic Research Foundation Grants 96-07-89323, 96-15-98333. V. Balashov is indebted to Marina Lebedeva for helpful and thoughtful discussion of numerico-mathematical points in code development. We also thank Greg Dipple, Peter Blattner, and an anonymous reviewer for their perceptive comments on a earlier version of the manuscript.

Appendix

Derivation of the diffusion part of the system of equations

The general transformation of diffusion coefficients for different reference systems is given by de Groot and Mazur (1984). To clarify eq (2) we give here the derivation of the relationship between the diffusion coefficients in the barycentric reference system and in the Fickian reference system for two-component fluid. In the barycentric reference system, the net diffusive mass flux of components is equal to zero

$$J_1^m M_1 + J_2^m M_2 = 0, \tag{34}$$

whereas in the Fickian reference system the net diffusive volume flux of components is equal to zero

$$J_1^v \overline{V}_1 + J_2^v \overline{V}_2 = 0. \tag{35}$$

In eqs (34, 35) the diffusive fluxes are defined in a similar manner

$$J_k^{RS} = -D_k^{RS} \nabla C_k, \tag{36}$$

where RS refers to either reference system. In general, the diffusion coefficients for each component in a two-component fluid are different, but in the Fickian reference system we have the same value for each because of the relation

$$\frac{\partial C_1}{\partial C_2} = -\frac{\overline{V}_2}{\overline{V}_1}. \tag{37}$$

We can relate barycentric and Fickian diffusive fluxes through:

$$\begin{aligned} J_1^v &= J_1^m + \mathscr{V} C_1, \\ J_2^v &= J_2^m + \mathscr{V} C_2, \end{aligned} \tag{38}$$

where $\mathscr{V}$ is the relative velocity of the barycentric reference system in the Fickian one. Substituting the fluxes from eq (38) into eq (35) and taking into account the thermodynamic relation

$$\overline{V}_1 C_1 + \overline{V}_2 C_2 = 1, \tag{39}$$

we arrive at an expression for $\mathscr{V}$

$$\mathscr{V} = -(J_1^m \overline{V}_1 + J_2^m \overline{V}_2). \tag{40}$$

Substituting this expression into (38), we have for the kth flux (k = 1, 2)

$$J_k^v = J_k^m - (J_1^m \overline{V}_1 + J_2^m \overline{V}_2) C_k. \tag{41}$$

Making use of eq (34) and eq (39) we can transform eq (41) into

$$\begin{aligned} J_1^v &= J_1^m \frac{\overline{V}_2}{M_2} \rho \\ J_2^v &= J_2^m \frac{\overline{V}_1}{M_1} \rho, \end{aligned} \tag{42}$$

where ρ is fluid density which is defined by

$$\rho = M_1 C_1 + M_2 C_2. \tag{43}$$

From eq (42) it is evident that for diffusion coefficients in the barycentric system we have

$$\begin{aligned} D_1 &= \frac{M_2}{\overline{V}_\rho^2} D^0 \\ D_2 &= \frac{M_1}{\overline{V}_\rho^1} D^0, \end{aligned} \tag{44}$$

where D^0 is the diffusion coefficient in the Fickian reference system.

For the barycentric system we can write the component mass balance equations as:

$$\frac{\partial \phi C_k}{\partial t} = \nabla \cdot (F D_k \nabla C_k) - \nabla \cdot (C_k \mathbf{q}) + \nu_k j^r, \tag{45}$$

where k = 1, 2 and F is the diffusion factor for a porous medium (Balashov, 1995) and takes into account such geometrical properties of pore network as the connectivity, the tortuosity, et cetera. Substituting the diffusion coefficients from eq (44) into eq (45) we arrive at the component transport equations, eqs (2) in the main text.

REFERENCES

Aagaard, P. and Helgeson, H. C., 1982, Thermodynamic and kinetics constraints on reaction rates among minerals and aqueous solutions: I. Theoretical considerations: American Journal of Sciences, v. 282, p. 237–285.

Balashov, V. N., 1995, Diffusion of electrolytes in hydrothermal systems: free solution and porous media, *in* Schmulovich, K. I., Yardley, B. W. D., and Gonchar, G. G., editors, Fluids in the Crust: London, Chapman & Hall, p. 215–251.

Balashov, V. N. and Lebedeva, M. I., 1991, Macrokinetic model of origin and development of a monomineralic bimetasomatic zone, *in* Perchuk, L. L., editor, Progress in Metamorphic and Magmatic Petrology: Cambridge, Cambridge University Press, p. 167–195.

—— 1996, On self-consistent model of chemical transport at metamorphism of rocks: Russian Academy of Sciences Doklady (Earth Sciences) (in press).

Balashov, V. N., Zaraisky, G. P., Tikhomirova, V. I. and Postnova, L. E., 1983, Diffusion of rock forming components in pore solutions at T = 250°C and P = 100 MPa: Geochemical International, v. 20, no. 1, p. 28–40.

Baumgartner, L. P. and Ferry, J. M., 1991, A model for coupled fluid-flow and mixed-volatile reactions with applications to regional metamorphism: Contributions to Mineralogy and Petrology, v. 106, p. 273–285.

Baumgartner, L. P. and Rumble, D., 1988, Transport of stable isotopes. I: Development of a kinetic continuum theory for stable isotope transport: Contributions to Mineralogy and Petrology, v. 98, p. 417–430.

Bickle, M. J. and McKenzie, D., 1987, The transport of heat and matter by fluids during metamorphism: Contributions to Mineralogy and Petrology, v. 95, p. 384–392.

Blattner, P. and Lassey, K. R., 1990, Transport of stable isotopes, kinetics, dispersive advection and the 'isotopic fronts' of Baumgartner and Rumble (1988): Contributions to Mineralogy and Petrology v. 105, p. 486–490.

Brace, W. F., Walsh, J. B. and Frangos, W. T., 1968, Permeability of granite under high pressure: Journal of Geophysical Research, v. 73, p. 2225–2236.

Connolly, J. A. D., 1997, Devolatilization-generated fluid pressure and deformation-propagated fluid flow during prograde regional metamorphism: Journal of Geophysical Research, v. 102, p. 18149–18173.

David, C., Wong, T., Zhu, W. and Zhang, J., 1994, Laboratory measurement of compaction-induced permeability change in porous rocks: implications for the generation and maintenance of pore pressure excess in the crust: PAGEOPH, v. 143, p. 425–456.

de Groot, S. R. and Mazur, P., 1984, Non-equilibrium Thermodynamics: New York, Dover Publications, Inc., 510 p.

Dullien, F. A. L., 1979, Porous Media, Fluid Transport and Pore Structure: New York, Academic Press, 396 p.

Holness, M. B. and Graham, C. M., 1995, P-T-X effects on equilibrium carbonate-H_2O-CO_2-NaCl dihedral angles: constraints on carbonate permeability and the role of deformation during fluid infiltration: Contributions to Mineralogy and Petrology, v. 119, p. 301–313.

Joesten, R. and Fisher, G. W., 1988, Kinetics of diffusion control mineral growth in the Christmas Mountains (Texas) contact aureole: Geological Society of America Bulletin, v. 100, p. 714-732.

Knipe, R. J. and McCaig, A. M., 1994, Microstructural and microchemical consequences of fluid flow in deforming rocks, *in* Parnell, J., editor, Geofluids: origin, migration and evolution of fluids in sedimentary basins: Geological Society of London Special Publication 78, p. 99–111.

Korzhinskii, D. S., 1936, Mobility and inertness of components in metasomatism: Akadadmy Nauk SSR Izvestia, series geology, v. 1, 36–60 (in Russian).

—— 1970, Theory of Metasomatic Zoning: Oxford, Clarendon Press, 162 p.

Labotka, T. C., 1991, Chemical and physical properties of fluids, *in* Kerrick, D. M., editor, Contact Metamorphism: Reviews in Mineralogy, v. 26, p. 43–104.

Lasaga, A. C., 1981, Transition state theory, *in* Lasaga, A. C. and Kirkpatrick, R. J., editors, Kinetics of Geochemical Reactions: Reviews in Mineralogy, v. 8, p. 135–169.

—— 1986, Metamorphic reaction laws and development of isograds: Mineralogical Magazine, v. 50, p. 359–373.

Lasaga, A. C. and Rye, D. M., 1993, Fluid flow and chemical reaction kinetics in metamorphic systems: American Journal of Science, v. 293, p. 361–404.

Lassey, K. R. and Blattner, P., 1988, Kinetically controlled oxygen isotope exchange between fluid and rock in one-dimensional advective flow: Geochimica et Cosmohimica Acta, v. 52, p. 2169–2175.

Lichtner, P. C., 1985, Continuum model for simultaneous chemical reactions and mass transport in hydrothermal systems: Geochimica et Cosmochimica Acta, v. 49, p. 779–800.

—— 1993, Scaling properties of time-space kinetic mass transport equations and the local equilibrium limit: American Journal of Science, v. 293, p. 257–296.

—— 1996, Continuum formulation of multicomponent-multiphase reactive transport, *in* Lichtner, P. C., Steefel, C. I. and Oelkers, E. H., editors, Reactive Transport in Porous Media: Reviews in Mineralogy, v. 34, p. 1–81.

Lichtner, P. C. and Balashov, V. N., 1993, Metasomatic zoning: appearance of ghost zones in limit of pure advective mass transport: Geochimica et Cosmochimica Acta, v. 57, p. 369–387.

Lichtner, P. C., Steefel, C. I. and Oelkers, E. H., editors, 1996, Reactive Transport in Porous Media: Reviews in Mineralogy, v. 34, 438 p.

Lüttge, A., and Metz, P., 1993, Mechanism and kinetics of the reaction: 1 dolomite + 2 quartz = 1 diopside + 2 CO_2: a comparison of rock-sample and of powder experiments: Contributions to Mineralogy and Petrology, v. 115, p. 155–164.

Oelkers, E. H., 1996, Physical and chemical properties of rocks and fluids for chemical mass transport calculations *in* Lichtner, P. C., Steefel, C. I., and Oelkers, E. H., editors, Reactive Transport in Porous Media: Reviews in Mineralogy, v. 34, p. 131–191.

Oelkers, E. H. and Helgeson, H. C., 1988, Calculation of the thermodynamic and transport properties of aqueous species at high temperature and pressure: Aqueous tracer diffusion coefficients of ions to 1000°C and 5 kb: Geochimica et Cosmochimica Acta, v. 52, p. 63–85.

Paterson, M. S., 1995, A theory for granular flow accommodated by material transfer via an intergranular fluid: Tectonophysics, v. 245, p. 135–151.

Rehbinder, P. A. and Shchukin, E. D., 1973, Surface phenomena in solids during the course of their deformation and failure: Soviet Physics Uspekhi, v. 15, No. 5, p. 533–554.

Rutter, E. H., 1976, The kinetics of rock deformation by pressure solution: Royal Society London Philosophical Transactions, ser A, v. 283, p. 203–219.

—— 1983, Pressure solution in nature, theory and experiment: Geological Society of London Journal, v. 140, p. 725–740.

Shklovskii, B. I. and Efros, A. L., 1976, Percolation theory and conductivity of strongly inhomogeneous media: Soviet Physics Uspekhi, v. 18, no. 11, p. 845–862.

Shmonov, V. M., Vitovtova, V. M. and Zarubina, I. V., 1995, Permeability of rocks at elevated temperatures and pressures, *in* Schmulovich, K. I., Yardley, B. W. D. and Gonchar, G. G., editors, Fluids in the Crust: London, Chapman & Hall, p. 285–313.

Shmulovich, K. I. and Shmonov, V. M., 1978, The tables of thermodynamic properties of gases and liquids, Issue 3, Carbon dioxide: Moscow, VNIIMS (All-Union Science-Researching Institute of Metrological Duty), 168 p. (in Russian).

Steefel, C. I. and Lasaga, A. C., 1994, A coupled model for transport of multiple chemical species and kinetic precipitation/dissolution reactions with application to reactive flow in single phase hydrothermal systems: American Journal of Science, v. 294, p. 529–592.

Steefel, C. I. and Lichtner, P. C., 1994, Diffusion and reaction in rock matrix bordering a hyperalkaline fluid-filled fracture: Geochimica et Cosmochimica Acta, v. 58, p. 3595–3612.

Tanner, S. B., Kerrick, D. M. and Lasaga, A. C., 1985, Experimental kinetic study of the reaction: calcite + quartz = wollastonite + carbon dioxide, from 1 to 3 kilobars and 500° to 850°C: American Journal of Science, v. 285, p. 577–620.

Thompson, J. B., 1959, Local equilibrium in metasomatic processes, *in* Abelson, P.H., editor, Researches in Geochemistry: New York, John Wiley & Sons, p. 427–457.

Walker, A. N., Rutter, E. H. and Brodie, K. H., 1990, Experimental study of grain-size sensitive flow of synthetic, hot-pressed calcite rocks, *in* Knipe, R. J., and Rutter, E. H., editors, Deformation Mechanisms: Rheology and Tectonics: Geological Society of London Special Publication 54, p. 259–382.

Weyl, P. K., 1959, Pressure solution and the force of crystallization: A phenomenological theory: Journal of Geophysical Research, v. 64, 2001–2025.

Yardley, B. W. D. and Lloyd, G. E., 1989, An application of cathodoluminescence microscopy to the study of textures and reactions in high-grade marbles from Connemara, Ireland: Geological Magazine, v. 126, p. 333–337.

—— 1995, Why metasomatic fronts are really metasomatic sides: Geology, v. 23, p. 53–56.

Zaraisky, G. P. and Balashov, V. N., 1995, Thermal Decompaction of Rocks, *in* Schmulovich, K. I., Yardley, B. W. D. and Gonchar, G. G., editors, Fluids in the Crust: London, Chapman & Hall, p. 253–284.

Zaraisky, G. P., Zharikov, V. A., Stoyanovskaya, F. M. and Balashov, V. N., 1986, Experimental investigation of skarn formation: Moscow, Nauka, 380 p.

Zhang, S., Paterson, M. S. and Cox, S. F., 1994, Porosity and permeability evolution during hot isostatic pressing of calcite aggregates: Journal of Geophysical Research, v. 99, p. 15741–15760.